PERFORMANCE OF FLEXIBLE EVAPORATOR FOR LOOP HEAT PIPE TECHNOLOGIES

By

MUKTA LIMAYE

A THESIS PRESENTED TO THE GRADUATE SCHOOL
OF THE UNIVERSITY OF FLORIDA IN PARTIAL FULFILLMENT
OF THE REQUIREMENTS FOR THE DEGREE OF
MASTER OF SCIENCE

UNIVERSITY OF FLORIDA

2007

ACKNOWLEDGMENTS

I would like to thank Dr. Klausner for his support and guidance throughout this project. His advice was crucial to help me keep up and keep on track. Many seemingly daunting experimental problems were solved through his suggestions.

I would also like to thank Pat Garrity and Richard Parker for their help in setting up the experimental facility and trouble shooting small and big problems that kept arising during the experiments. Many innovative ideas have sprung out from discussions with Pat and Richard. Finally I would like to thank my parents and my family for their support and encouragement throughout my master's studies.

TABLE OF CONTENTS

page

LIST OF TABLES

LIST OF FIGURES

LIST OF ABBREVIATIONS

LHP:	Loop heat
$\dot{q}''$	Heat flux rate
$\Delta P_{cap,\max}$	Maximum capillary pressure
P	Pressure
σ	Surface tension
r_{eff}	Radius of curvature at liquid-vapor interface
k_{eff}	Effective conductivity of porous wick
ΔT_b	Boiling superheat
t_{wick}	Wick thickness
h	Heat transfer coefficient
$\dot{m}_{wick}$	Wicking mass flow rate
c_p	Specific heat
T	Temperature
h_{fg}	Latent heat
u	Velocity of fluid
K	Permeability of porous material
μ	Viscosity
θ	Contact angle

Subscripts:

v	vapor
l	liquid

sat	saturation
in	inlet
est	estimate

Abstract of Thesis Presented to the Graduate School
of the University of Florida in Partial Fulfillment of the
Requirements for the Degree of Master of Science

PERFORMANCE OF FLEXIBLE EVAPORATOR FOR LOOP HEAT PIPE TECHNLOGIES

By

Mukta Limaye

December 2007

Chair: James F. Klausner
Major: Mechanical Engineering

In this study a flat, flexible evaporator, which can conform to contoured surfaces, has been investigated for loop heat pipe applications. A loop heat pipe (LHP) is a passive, two phase heat transfer device comprising a porous membrane in its evaporator. It is observed that the performance of the LHP is largely governed by the wicking characteristics of this porous membrane. A number of flexible membranes have been tested. The highest wicking rate is observed for a membrane made of 20 layers of dressing gauze. This is a result of its large pore size and the high wettability of the cotton fabric. The heat transfer performance of this membrane is first tested in a rigid evaporator. A maximum heat flux of 5.95 W/cm^2 and maximum heat transfer coefficient of 2865 W/m^2K are measured. Other membranes tested were cellulose sheet, polyethylene sheet and blotting paper and maximum heat fluxes of 0.43 W/cm^2, 1.5 W/cm^2 and 2.9 W/cm^2 respectively were measured. The maximum heat transfer coefficients measured for these membranes were 551 W/m^2K, 876 W/m^2K and 2100 W/m^2K respectively. The dressing gauze membrane has been selected for fabricating a flexible evaporator. The flexible evaporator is fabricated using heat sealable, flexible barrier pouch and the dressing gauze membrane is inserted inside it. The maximum measured heat flux for the flexible evaporator, without reaching dryout, is 3.2 W/cm^2 and maximum measured heat transfer coefficient is 1165 W/m^2K. The

mechanism of heat transfer in this system is boiling. Vapor bubbles formed in the membrane lower its wicking rate as well as its heat transfer performance. Also, poor contact between membrane and evaporator yields higher wall temperatures. Thus, ensuring efficient vapor removal while maintaining a good contact between membrane and evaporator is a significant challenge in the design of such a flexible system.

CHAPTER 1
LITERATURE REVIEW

Heat Pipe

A heat pipe is a passive heat transfer device that can transfer a very large amount of heat over short distances with a small temperature difference between the heat source and heat sink. It is comprised of an evaporator section, a condenser section and a short adiabatic section connecting the two. The heat pipe uses a porous wick across which evaporation and condensation takes place. The capillary forces developed at the liquid-vapor meniscus within the wick pores drive the fluid through the system, and no mechanical pumping is required. Hence it is a passive heat transfer device. It is reported that the first heat pipe was developed in 1964 at the Los Alamos National Laboratory. It was made of a sealed metal tube, (19 mm diameter and 0.9 m long), lined with porous stainless steel screen mesh and used liquid sodium as the working fluid [1]. It could transfer up to 1000W power at about 875^0C. It was observed that the temperature throughout the length of the heat pipe remained almost constant at steady state operation. As heat pipes transfer a large amount of heat with a small driving temperature difference, their bulk conductivity is typically 4 to 5 orders of magnitude higher than a copper rod [2]. This makes them very attractive for cooling and thermal management applications.

The main principle behind the operation of heat pipes is the capillarity. When liquid evaporates through a porous medium in the evaporator section of heat pipe, capillary forces are developed at the liquid-vapor meniscus. These forces enable the interface to withstand a pressure difference between the liquid and vapor phases. This pressure difference provides the pumping required for flow of fluid in the heat pipe. The “capability of the interface between the liquid and vapor in a fine pored structure to withstand a pressure difference across the interface” is known as capillarity [2]. The vapor generated in the evaporator section flows towards the condenser

through the adiabatic section. At the condenser section, the vapor is condensed back to liquid. This liquid flows back to the evaporator through the wick by capillary action. Most heat pipes use a liquid that 'wets' the porous medium. This means that the adhesive forces between the porous material and the liquid are stronger than the liquid cohesive forces. Hence the contact angle is lower than 90^0 and greater pressure can be created by the surface tension forces.

The maximum heat that can be transferred by a heat pipe is subjected to various limits. These limits are discussed below.

1. Capillary Limit: The maximum capillary pressure that can be developed across the liquid-vapor interface for a given fluid-wick combination can be expressed as shown in Eq. 1-1. As long as the total pressure drop in the system, from the vapor and liquid line flow is lower than $\Delta P_{cap,max}$, the normal operation of heat pipe will be achieved. As the heat input to the evaporator is increased, the mass flow rate of vapor will increase and pressure drop in the system will increase. When the system pressure drop exceeds the maximum capillary pressure, the meniscus at the interface is destroyed. The porous wick can no longer supply liquid to the evaporator at the rate of evaporation and hence dry out in the evaporator is observed. The evaporator temperatures rise sharply and the heat pipe cannot function. Maximum flow is obtained when the system pressure drop is exactly equal to the maximum capillary pressure. The corresponding heat input is the maximum heat that can be transferred by the heat pipe before reaching dryout and is known as the capillary limit.

$$\Delta P_{cap,\max} = P_v - P_l = \frac{2\sigma}{r_{eff}} \tag{1-1}$$

2. Boiling Limit: Surface irregularities of the evaporator wall typically produce many nucleation sites. Vapor can be trapped at these sites. As long as the difference between vapor pressure inside the bubble and the liquid pressure outside the bubble is less than the surface tension forces at the bubble-liquid interface, the vapor will not escape. However, if the difference exceeds the surface tension, vapor bubbles will rise from the nucleation site and boiling will commence. The presence of porous material complicates the determination of the radius of nucleation sites. The heat flux at which boiling will occur can be expressed by Eq. 1-2. The consequences of operating a heat pipe above the boiling limit depend largely on the design and performance factors, the working fluid used etc. For example, in the case of liquid metal working fluids, the superheat required to commence boiling is very large and hence the boiling limit is very high. If boiling commences at moderate heat flux, vapor bubbles may be formed at various locations in the wick, thus increasing the liquid pressure drop and lowering the capillary limit. For a configuration in which the heater is placed below the evaporator, the bubbles formed at the evaporator wall will rise through the wick and enter the vapor space. Here, the liquid-vapor interface will be repeatedly broken and reformed. At high boiling

rates, the capillary forces will be unable to reform the meniscus and dryout will occur. In addition, the presence of vapor bubbles in the wick will restrict the flow of returning liquid from the condenser resulting in evaporator dryout.

$$q_b = \frac{k_{eff} \Delta T_b}{t_{wick}} \qquad (1\text{-}2)$$

3. Entrainment Limit: In a heat pipe the vapor and liquid phases are moving in opposite directions across the wick. Owing to its lower density, the velocity of vapor can be much greater than the liquid. Thus the vapor exerts a shear force on the liquid. At high heat flux, the vapor velocities can be very high and cause some of the liquid at the interface to be entrained with the vapor. This will occur when the shear force exceeds the surface tension force. This phenomenon is usually observed at the evaporator near the exit of a uniform cross section heat pipe where the vapor mass flow is the highest. Due to entrainment of liquid in the vapor line, the rate of loss of liquid from evaporator region is greater than replenishment form the condenser. Hence dryout occurs.

4. Sonic Limit: The sonic limit is reached when the applied heat input is such that the vapor flow near the evaporator exit is choked. Once the flow is choked, the vapor flow cannot be increased unless the vapor temperature rises, resulting in a drop in vapor density. Hence, when the input is increased beyond the sonic limit, the evaporator temperature rises to a new point such that the vapor flow is choked again. Thus, the heat pipe operation can still be sustained without dryout even if the sonic limit is exceeded. However, the sonic limit increases rapidly with temperature. Hence, higher and higher temperatures will be obtained and cooling may not be effective. Also, the heat pipe may no longer be isothermal throughout its length.

Loop Heat Pipe

Introduction

A loop heat pipe (LHP) is a modification to the conventional heat pipes described above, in certain aspects (Figure 1-1). First of all, the porous wick is present only in the evaporator section of a LHP. The evaporator and condenser are typically connected by long, smooth vapor and liquid lines that are well insulated. In addition, the LHP comprises a fluid reservoir, also known as a compensation chamber. This provides the fluid inventory necessary for the LHP to respond to the changes in input heat loads. The compensation chamber is thermally and hydrodynamically connected to the evaporator. It is a two-phase reservoir and plays a key role in determining the pressure and temperature of LHP operation [3]. Compared to the conventional

heat pipes, the LHPs can transfer heat over much larger distances, typically a few feet. Also, they can operate under adverse elevation conditions i.e. when the condenser is located below the level of the evaporator. The gravity-independent operation of these devices is of particular significance in space applications [4].

The thermodynamic cycle performance of loop heat pipe (Figure 1-2) was explained by Cheung et al. [5]. Vapor at point 1 is saturated vapor in the evaporator vapor grooves which becomes slightly superheated until it reaches the evaporator exit (point2). Point 3 can be considered the vapor state at the condenser inlet. The vapor is condensed from point 4 to 5 and then subcooled to 6. The subcooled liquid is then returned to the compensation chamber via liquid line 7-8. Due to the pressure drop of the liquid in the porous wick, it attains state 9 at the evaporator and the thermodynamic cycle is completed. The pressure difference between point 9 and point 1 is maintained by the capillary forces acting at the vapor-liquid interface. It is noted that the first successful LHP was developed and tested by Maydanik et al. in 1972 [4]. It used water as working fluid and was capable of transferring up to 1 kW through distance of about 1.2 m.

Numerical Studies for LHP Performance

Many numerical investigations have been performed by various researchers to study different aspects of the LHP performance. Kaya and Hoang [6] developed a model based on an energy balance for each component of a LHP. Their aim was to develop a simple, quick model that could be used for parametric studies in the designing of future LHPs. The main assumption was that of heat and mass flows in the radial direction only. Further it considered the presence of both phases in the compensation chamber, thereby accounting for incomplete condensation of vapor in the condenser. The total pressure drop in the LHP was determined from the pressure drops in individual components. Then the temperature drop across the wick was estimated, by

calculating the pressure drop in the wick and considering the liquid to be saturated at both ends of the wick. The heat conducted through the wick from evaporator to the compensation chamber (known as heat leak) is a function of this temperature drop. For the energy balance of the compensation chamber, this heat leak was balanced by the heat exchange with the ambient and heat supplied to the returning subcooled liquid. A similar analysis was performed on other components of the system. Two different correlations were used to estimate the effective thermal conductance of a porous wick. And the difference in the results was noted. The pressure drop in the system was modeled with the assumption of single phase flow in the condenser and subcooler. For the vapor grooves, both laminar and turbulent regimes were considered. The capillary limit of heat transfer was modeled to occur when the total pressure drop in the system is equal to the capillary pressure created by the wick at the liquid-vapor interface. The model was validated using ammonia as a working fluid and two different evaporator configurations having a sintered nickel wick with pore radius approximately 1.2 μm. During the validation tests, the condenser temperature was first set to a desired value and heat was applied to the evaporator. Steady state performance of the LHP was recorded. Some power cycling tests were also performed. These investigators did not reach the heat transfer limit due to the heater power limitation. The value of heater limit has not been mentioned in the paper. However, partial dryout of the primary wick was experimentally observed at higher heat flux, even before the capillary limit was reached. This phenomenon was not predicted by the mathematical model. They also observed that at low power levels, the evaporator temperature decreased with increasing the heat input. This is because at lower power, the heat losses to the ambient from the compensation chamber are significant. The increase in input heat flux discharges additional cold fluid from the condenser into the compensation chamber. The effect of heat leak is reduced by

these two factors, resulting in a colder fluid entering the evaporator and causing a drop in temperature. This is known as the 'variable conductance mode' of LHP operation. As the heat flux is increased further, the heat leak dominates and the evaporator temperature increases with heat input. This is the 'constant conductance mode'. Results from other sets of experiments show that increasing the condenser temperature increased the evaporator temperature of the LHP.

Kaya and Goldak [7] numerically investigated the boiling limit in a wicked evaporator having vapor grooves. The spaces between the grooves (called fins) were in direct contact with a wick having 7.2μ diameter pores and 60% porosity. This model assumed local thermal equilibrium between the fluid and wick and retained the convective terms in the energy equation. It could predict the LHP performance for 2 operating regimes: 1) single phase liquid in the wick and 2) vapor formation in parts of the wick just below the fin. The mass, momentum and energy equations are solved by applying appropriate boundary conditions. This model predicts an increase in pressure with input heat flux. It also predicts the variable conductance and constant conductance modes of the LHP. The authors estimate the boiling limit from the theory proposed by Mishkinis and Ochterbeck in [8]. As per this theory, the rate of nuclei formation is a function of heat flux, wick thickness and pore size. When this heat flux is such that nuclei formation rate equals the rate at which liquid is replenished to the heated wick, the boiling limit is said to be attained. However, experimentally it was observed that dryout was not obtained for heat fluxes almost twice that predicted by the boiling limit calculation. The authors have reasoned that even after nucleate boiling commences in the wick, the meniscus is not destroyed as the vapor has an escape path through the vapor grooves. Also, the increasing vapor region under the fin exerts greater pressure on the liquid under the meniscus and impedes boiling. Hence LHP operation can

be sustained at higher heat fluxes. It was also noted that the non condensable gases encourage boiling and good contact between fin and wick enhances LHP performance.

Experimental Studies for LHP Performance

Many different design concepts for Loop Heat Pipes and the effect of various parameters on their performance have been investigated experimentally by various researchers. Riehl and Siqueira [3] experimentally investigated the effect of the compensation chamber geometry on the LHP performance. They studied two ammonia filled stainless steel LHPs with polyethylene wicks. LHP1 had a larger compensation chamber than LHP2. Both were filled with liquid to 50% of their volume. The dimensions of evaporators were such that the evaporator inlet of LHP1 was completely submerged in the liquid of the compensation chamber. Whereas LHP2 had a part of the evaporator inlet subject to the vapor from the compensation chamber. It was noted that for the rated power of 80W, the compensation chamber temperature for LHP1 was 38.3^0C while that for LHP2 was 56.5^0C. The corresponding evaporator temperatures were noted to be 75.5^0C and 85^0C respectively. Thus it was concluded that there was better coupling between the evaporator and compensation chamber in the case of LHP2. LHP2 had a lower thermal resistance than that of LHP1. This results in more loss due to heat conducted to the compensation chamber. This can be rectified by having a geometric transition coupling between the two. It will increase the thermal resistance between evaporator and compensation chamber, leading to lower wall temperatures on the evaporator. The researchers noted that no temperature oscillations were observed during any of the tests. The effect of non condensable gases was also studied on the two LHPs. It was observed that the performance of the LHP1 remained unaffected by non condensable gases, whereas the LHP2 developed start up transients. However they were suppressed over a period of time and did not influence the steady state operation of LHP2. Similar results were obtained when the experiments were repeated with acetone, suggesting that

acetone could replace ammonia in similar applications. In both the LHPs, temperature overshoot was observed as a result of sudden large change in input power. It has been explained as the result of the sudden flow of cold liquid into the compensation chamber when the input power is changed in a large step.

This phenomenon is termed as 'cold shock'. It was further investigated by Nikitkin et al. [9]. The evaporator wall temperature overshoot was noted when there was a sudden change in the input power or the sink temperature. It was more pronounced in the case of larger LHPs with bigger condensers. When the heat input to a LHP is suddenly increased, the cold liquid from the condenser is displaced by the incoming vapor and is dumped into the compensation chamber. This causes a drop in its pressure and temperature. As a result, the pressure drop in the system increases temporarily. If the pressure drop is now greater than the capillary pressure, instantaneous dryout is obtained and wall temperatures overshoot. Nikitkin et al. also observed a small drop in the compensation chamber temperature corresponding to the temperature overshoot in the evaporator. Further, they note that during the large step change in heat input, the liquid line temperature becomes momentarily equal to the vapor line temperature. It is indicative of back flow of vapor in the compensation chamber and leads to temporary evaporator dryout. To rectify the problem of overshoot, it was recommended that the liquid line should be insulated to prevent subcooling in the condenser.

In another study, Kaya and Ku [10] tested a small LHP. It was made of 10 mm inner diameter aluminum tube with a 3 mm thick nickel wick. Nominal pore size of the wick was 1.2 μ and 60% porosity. Ammonia was used as a working fluid. Successful start up was obtained for input power as low as 5W. This is significant for space applications where auxiliary heating of the compensation chamber may not be feasible. However, temperature overshoot was observed

at the start up, most likely due to the 'slow movement of the cold liquid from the condenser' [10]. These researchers also noted the two regimes of variable conductance and constant conductance in the operation of this device. Some power cycling tests were also performed and the LHP exhibited steady operation under those conditions. Even under rapidly decreasing input power and heat sink temperatures, the LHP operation was not negatively affected. However, temperature hysteresis was observed during power cycling tests. The authors suggest that it may be due to the void fraction in the evaporator core and needs further investigation.

Wirsch and Thomas [11] experimentally investigated the performance of ammonia LHP with a nickel wick having 70% porosity. In these experiments, the vapor temperature was the controlled parameter. Tests were performed for two controlled vapor line temperatures of 40^0C and 50^0C. No dryout was observed in the former case but for a vapor line temperature of 50^0C, the dryout was obtained at an input power of 337 W. It was concluded that the capillary limit was reached for this LHP. The maximum heat transfer coefficient obtained in this test was 6.285 kW/m^{2}K and the critical heat flux was noted to be 12.6 W/cm^2.

Wick Characterization Studies

Many important characteristics of the LHP, such as maximum heat transfer limit, are determined by the wick used in the evaporator. The performance of the wick depends on many parameters such as its conductivity, porosity, pore size thickness etc. Selecting the correct wick is an important part of LHP design. Li et al [12, 13] have experimentally evaluated the effects of three parameters on the wick performance: wick thickness, volumetric porosity and pore size. They used multi-layered sintered copper wicks with thickness less than 1mm. The porosity of wicks tested was about 70% and pore size 56 μ. The wick was bonded to a test section heated from below. The water level in the wick was maintained constant by flow from a reservoir. Distilled water was used and tests were carried out under atmospheric conditions. A cartridge

heater was used to supply heat to the wick from below. The values of critical heat flux and heat transfer coefficients obtained in these tests are the highest reported in open literature---367.9 W/cm^2 and 245.5 kW/m^2K respectively. The authors note that the critical heat flux increases with increase in the thickness and mesh size but is independent of the volumetric porosity. Also, for a given porosity and pore size, the heat transfer coefficient was found to be independent of the thickness. For a given wick, the heat transfer coefficient initially increased with increase in input heat flux and then decreased. This shows that the LHP operation was sustained even at partial dryout. The authors also visually observed boiling at higher heat flux. They noted that the LHP can operate even when the porous medium contains both phases, as long as the vapor bubbles can escape into the vapor space. Another important result of these tests was that good contact between the evaporator and wick yields better heat transfer performance of the wicks. It was noted that bad contact resulted in superheat temperatures that were higher than that for pool boiling. Based on the data collected from all their experiments, the authors have proposed a boiling curve for thin sintered metal wicks (Figure 1-3). It is comprised of 3 main regimes. At low heat flux the heat is transferred by convection and wall temperature increases rapidly with small increases in heat flux, resulting in low heat transfer coefficient. As the heat flux is increased further, the wall temperature is observed to suddenly drop. This is the start of the nucleate boiling regime. The inception heat flux depends on the pore size and wick thickness. In this regime wall temperature increases slowly with large increases in heat flux and very high values of heat transfer coefficient are obtained.

This regime is characterized by the formation of bubbles on the wall and wick that rise through the wick into the vapor space. The final regime observed was the thin film evaporation regime, in which the meniscus receded further in the wick and liquid evaporates directly from the

heated surface. This gave the best heat transfer performance until dryout was obtained. An important conclusion of the authors was that nucleate boiling can enhance the heat transfer performance in the porous wicks and that the capillary limit is determined by the minimum meniscus radius. This meniscus could be formed in either the vertical or horizontal direction in the wick or between the wick and the evaporator wall.

Hanlon and Ma [14] performed a similar study with the aim of optimizing the wick parameters so that evaporation could be obtained only at the liquid-vapor interface. Their set up was similar to the one in [12] with a sintered wick secured in a housing in which the water level was maintained by flow from external tanks. The evaporation was carried out under atmospheric conditions and the only resistance to the flow was due to the porous wick. The main hypothesis of this study was that for thin wicks, the heat will be conducted from the evaporator wall through the metallic wick to the liquid-vapor interface, where evaporation will take place. Hence as long as boiling in the wick is avoided, the supply of water to the heated surface will not be hampered by the vapor bubbles in the pores and very high heat transfer coefficients could be obtained. Furthermore, they predicted the superheat required for the onset of nucleate boiling to be inversely proportional to the pore size. Thus a small pore size would lead to greater boiling as well as capillary limits. However, the permeability would decrease as pore size is reduced. The numerical model set up by the authors calculated the temperature profile in the wick by solving the pressure, temperature and energy equations, for given wick parameters. If the superheat at any point exceeded the boiling superheat, the heat flux was reduced until no boiling was obtained. This determined the boiling limit. Then the capillary limit was determined for the same operating parameters by equating the capillary pressure developed in the wick to the pressure drop in the wick. The same procedure was repeated for a range of different wick thickness. For

the range of thickness considered, the boiling limit was lower than the capillary limit and was expected to cause dryout. However, experimental findings showed that the wicks could withstand nucleate boiling without drying out, and the heat transfer coefficients were lower than those predicted by the model. These researchers also noted an increase in heat flux required for the inception of boiling with an increase in wick thickness. Nucleate boiling resulted in an almost constant slope of wall superheat vs. heat flux for these experiments.

In all the experiments cited above, the wetting of the wick was always ensured by some external mechanism, like flow from a reservoir etc which is independent of the wicking ability of the membrane.

In another study performed with microchannel polymer membranes, Wang and Peterson [15] experimentally studied the performance of polymer films having trapezoidal channels for heat pipe applications. Methanol was used as the working fluid due to its better wettability for the polymer film. The film was bonded to an aluminum plate and heated in a vacuum chamber. The pressure in the chamber was maintained at the saturation pressure corresponding to the temperature of the liquid in the compensation chamber. One end of the membrane was immersed in a tank filled with methanol and maintained at constant temperature. The other end of the membrane was heated with a heater of size 6.4 cm^2. The effects of two parameters were studied – tilt angle of the film and the total length of the film. The results showed that the critical heat flux decreased rapidly with increasing the length of the membrane and the tilt angle. In these tests a maximum heat transfer coefficient of 5 kW/ m^2K was recorded and maximum heat flux was 2.17 W/cm^2 at a tilt angle of 5^0. Further, the effect of channel geometry was also modeled and it was concluded that for a fixed top width, reducing the base width of the channel results in an increase in the maximum heat flux.

Visual Studies

Wang et al. [16] performed a visual study of boiling in porous media. They used 7mm diameter glass beads packed closely in a container filled with water and heated from bottom. The process was recorded by a CCD camera. The heat flux range in these experiments was 1.61 W/cm^2 to 12.13 W/cm^2. Tests were carried out under atmospheric conditions. At heat fluxes up to 3.68 W/cm^2, small bubbles were formed at some bead-wall contact points. Most of the space was filled with water and the wall superheat was less than 2^0C. As the heat flux was increased, the nearby bubbles coalesced to form larger bubbles, called primary bubbles, which grew in size with increasing heat input. At higher heat flux, the growth of the bubbles was constrained by the pore spaces (regions between the beads). Bubbles larger than the pore space got truncated at the neck and escaped to vapor space. It was observed that the heated surface was constantly replenished by surrounding water, thus keeping wall superheats to within 4 to 5^0C. This process of bubble growth and collapse became more rapid with increasing heat flux until finally the pore spaces were mostly filled with vapor. Although the wall-bead contact region could still be wetted, the wall temperatures became very unsteady. The authors concluded that the size of spaces formed between the beads and wall was small and hence facilitated the replenishment of water. This parameter would mainly determine the dryout.

Innovative Designs of Heat Pipes

Most conventional heat pipes and loop heat pipes as described above have a circular cross section. In most applications, they have to be connected to the heat source through a connector such as a saddle. This adds to the total resistance of the system and creates more issues with contact resistance. To overcome this problem, many studies have focused on developing flat prototypes for heat pipe and loop heat pipes [17-24]. Moreover, from the perspective of applications in cooling of electronics, it has been desired to have these devices in miniature sizes.

Maydanik et al. [17] have defined 'miniature' loop heat pipes as having evaporator diameter of less than 8 mm and liquid and vapor line diameters of 3 mm or less. The active length of such an evaporator is about 10-15 mm. They investigated various designs of miniature loop heat pipes (Figure 1-4).

The LHPs consisted of sintered metal wicks in the evaporator section. The wicks had pore sizes of 1-10 μm and porosities of 60% to 70%. Maximum heat flux as high as 69 W/cm^2 and heat transfer coefficient of 31.7 kW/m^2K were recorded for a copper heat pipe using copper wick and water as the working fluid. It was noted that even higher heat flux rates could be transported if the condenser cooling intensity was increased. Similar results have been documented by Singh et al. [18] using an air cooled condenser. They designed a flat disc shaped evaporator with effective vapor removal channels and were able to attain high heat fluxes and heat transfer coefficients.

Wang and Peterson [19] designed and tested a flat heat pipe of dimensions 152.4 X 25.4 X 2.71 mm (Figure 1-5). The inner surface of the heat pipe was layered with sintered screen mesh and round wires were placed between them at equal intervals to form vapor spaces.

The center to center distance between the wires (denoted by S_w in the Figure 1-6) was about 2 mm. Water was used as working fluid in these tests. Various parameters such as mesh size, wire diameter, tilt angle and wick thickness were studied. The heat transfer limit was analytically determined by considering the capillary limit, boiling limit and entrainment limit for various cases. The dryout heat flux was estimated to be the lowest of these limits. The results of the experiments are in close agreement with the analytical predictions. However, the authors do not explicitly mention the limiting cause for heat transfer capacity in each test. So it cannot be

determined from the published work whether the capillary, boiling or entrainment limit of the heat pipe was reached. These designs resulted in a maximum heat flux of up to 19.1 W/cm^2.

Sauciuc et al. [20] used 'super fiber bundle' wicks in their design of heat pipe for applications to notebook computers. They have realized that there are two competing factors involved in wick selection. High permeability is required to lower the resistance to fluid flow and this can be achieved by an increase in the pore size of the wick. However, to be able to sustain high pressure drop in the heat pipe, the wick should have small pores that can generate a very high capillary pressure. Particularly, for the notebook cooling applications, high capillary pressure is desired to be able to operate with the evaporator section of the heat pipe placed above the condenser section (top heating mode operation). The super fiber bundles designed by these researchers exhibit greater permeability than the sintered meshes. But they also have a higher pumping capacity than the grooved or wrapped mesh heat pipe. Tests were conducted for all 4 wick types (grooved, wrapped mesh, sintered and fiber bundle) in the top heating mode. Super fiber bundle heat pipe was observed to have the least thermal resistance which remained constant up to 4.25 W/cm^2. Grooved heat pipe was seen to have the highest thermal resistance due to its large pore size which results in a low capillary limit. The thermal resistance of the sintered wick heat pipe was higher than that of super fiber bundle because of its smaller pore size and low permeability.

In another work, Tsai [21] et al. designed a flat evaporator with the compensation chamber, evaporator and vapor chamber integrated into a single plate (Figure 1-7). The 'comb grooves' act as capillaries and draw the fluid vertically up from the compensation chamber. It is evaporated as it passes through the grooves and vapor is let into the vapor chamber from where it is removed to the condenser by vapor line. A copper screen mesh prevents the vapor from flowing back

towards the compensation chamber. The maximum heat removed was approximately 80 W and the heater area can be approximated to be 1.95 cm^2 from the information provided in the paper, resulting in a maximum heat flux of 35 W/cm^2. The working fluid for these tests was methanol.

Shimizu et al. [22] have reported some experimental results on flexible heat pipe using carbon fiber wick. Their design of heat pipe comprises of stainless steel evaporator and condenser sections connected by bellows. This enables the condenser section to be oriented at different angles with respect to the evaporator. The wick used was made of bundles of flexible carbon fiber filaments. The wick was placed along the entire length of the heat pipe. Acetone was used as the working fluid in these tests. The heat pipe was tested in various modes--- the angle between the evaporator axis and condenser axis was varied for each mode. The heat pipe could transfer up to 1.5 W/cm^2 (201W) in vertical orientation with maximum evaporator temperature of only 60 ^{0}C. However, when the condenser level was below that of the evaporator the overall heat pipe resistance was higher.

Savino et al. [23] note that the surface tension of fluids decreases with increase in temperature. This tends to inhibit the return of fluid from the condenser to the evaporator section of heat pipes. To over come this problem, they used the 'Self-rewetting fluids' developed by Abe [24-25] in Japan. These fluids are mixtures of water and butanol or higher alcohols. They exhibit an increasing surface tension with increase in temperature. In addition, due to the different vaporization properties of alcohol and water, a concentration gradient is created in the heat pipe. This assists the return of condensate by virtue of Marangoni flow. These mixtures were tested in conventional, grooved copper heat pipes. Whereas water heat pipes reached dryout at input power of 4 W, a similar heat pipe using the binary mixture had a dryout limit of up to 8 W. The researchers also tested wickless heat pipes in horizontal as well as vertical orientation. In the

vertical set up (with evaporator below the condenser section), both heat pipes had similar temperature profiles. This was because the gravity effects dominated the return of fluid to the evaporator. However, for horizontal set-up it was seen that the heat pipe with a binary mixture had almost twice the thermal conductance as that of the water heat pipe. The temperature profile in the binary fluid heat pipe was more uniform as compared to the water heat pipe. From these results it is evident that 'self- rewetting fluids' are an attractive choice for space applications. Abe [25] has conducted experiments in parabolic flights with these fluids. The heat pipes built for these tests were made of flexible polyamide panel containing tubes filled with the binary fluids. Steady operation was observed in low gravity conditions. Further detailed results from these tests are not yet available.

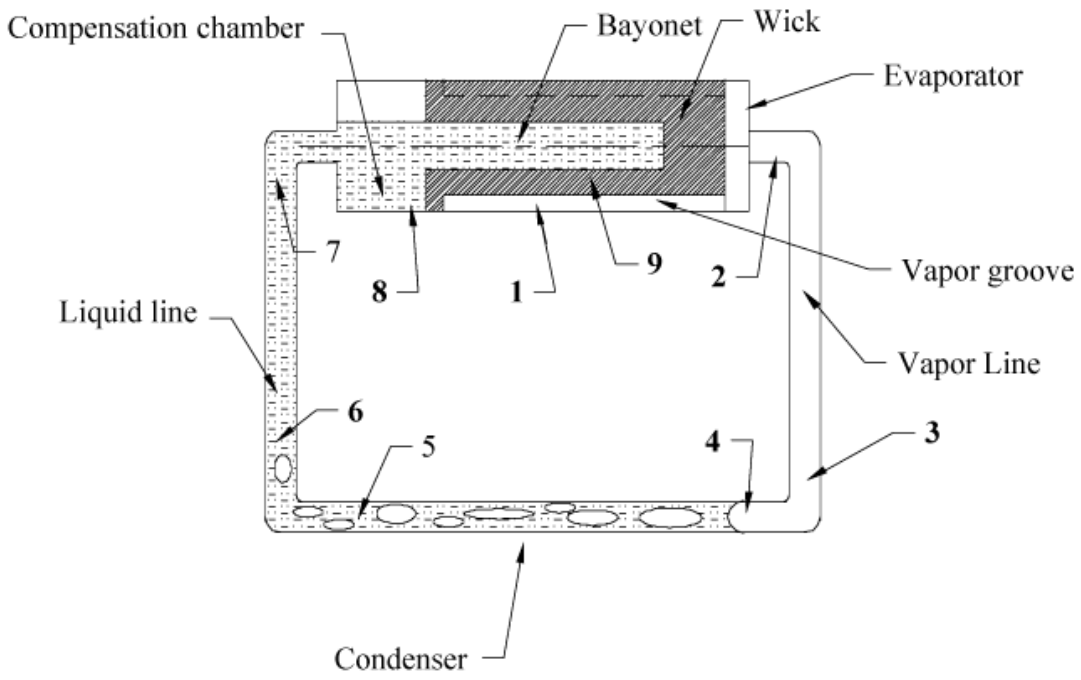

Figure 1-1: Schematic of a Loop heat pipe

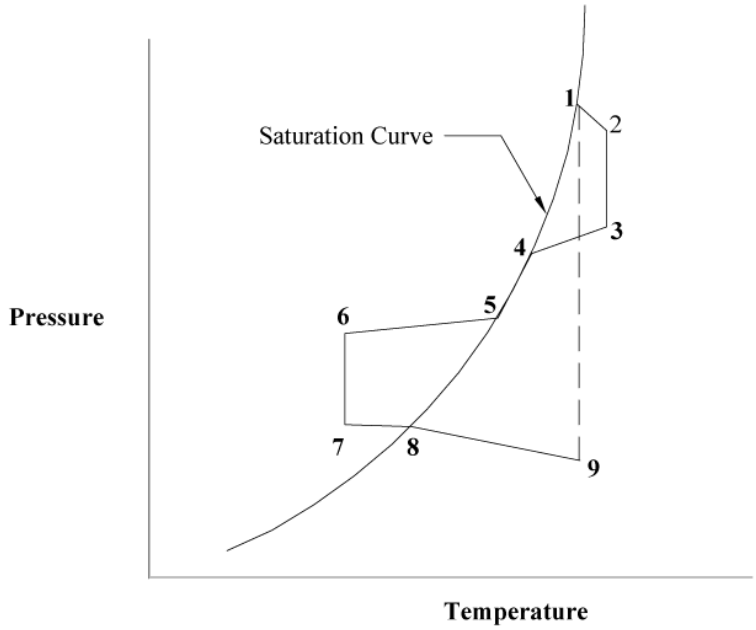

Figure 1-2: Thermodynamic cycle for LHP operation

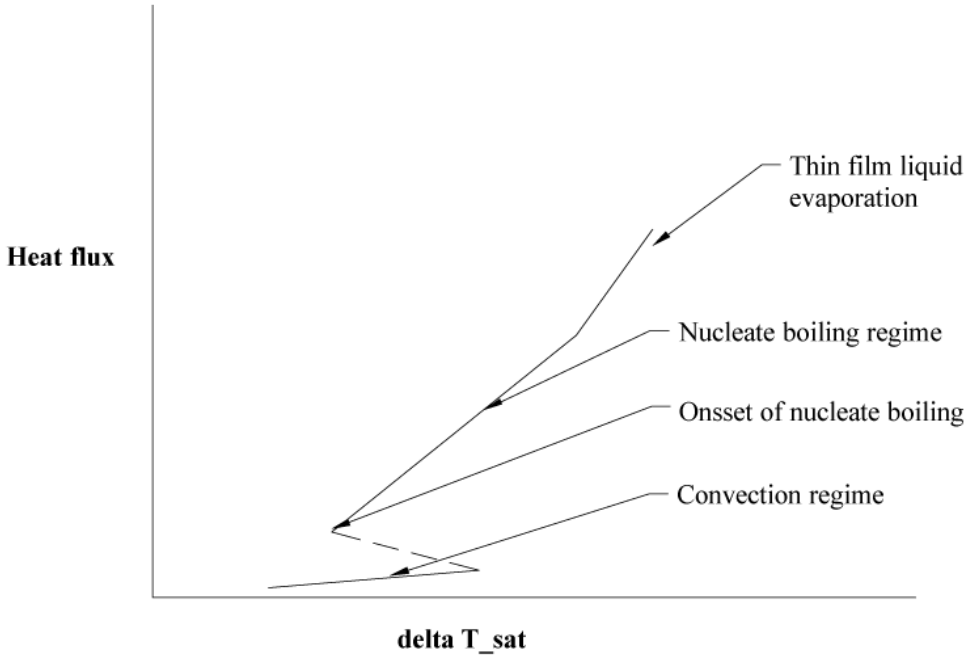

Figure 1-3: Boiling curve for thin wicks as proposed by Li and Peterson

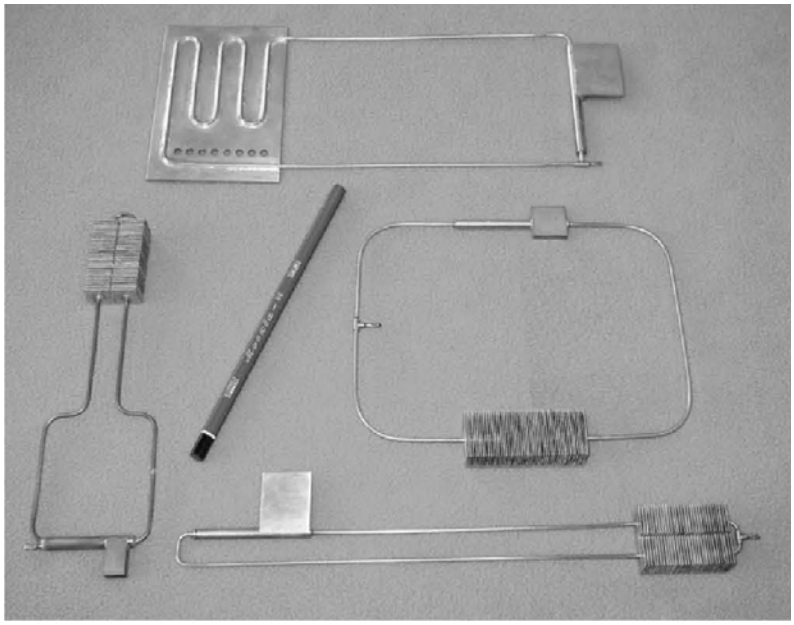

Figure 1-4: Various designs of flat loop heat pipes tested by Maydanik et al. [adapted from Maydanik, Y., Vershinin, S., Korukov, M., and Ochterbeck, J., "Miniature Loop Heat Pipes---A Promising Means for Cooling Electronics," IEEE Transactions on Components and Packaging Technology, Vol. 28, No. 2, 2005, pp.290-296. This figure appears as Fig 3 on page 292 in the reference.]

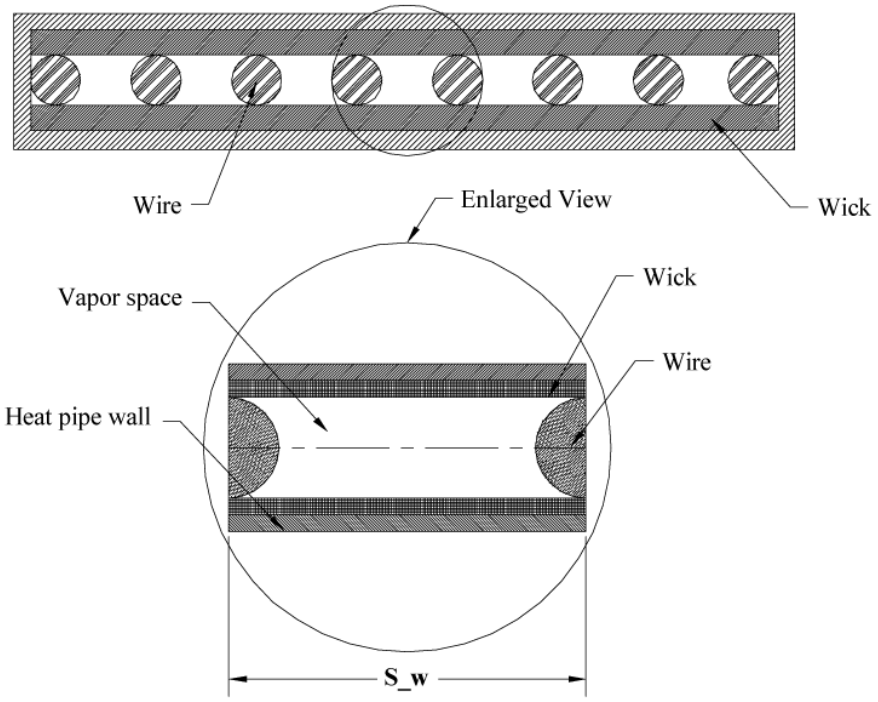

Figure 1-5: Wick structure for the flat heat pipe designed by Wang and Peterson

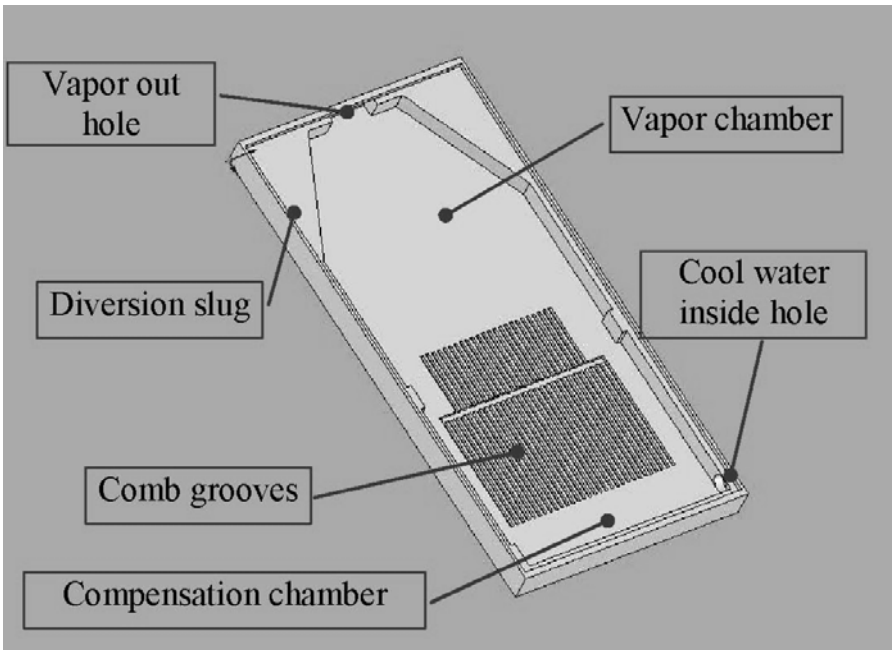

Figure 1-6: Flat integrated evaporator design for flat loop heat pipes [adapted from Tsai, M., Yu, C., and Kang, S., "Flat Plate Loop Heat Pipe with a Novel Evaporator Structure," *21st IEEE SEMI-THERM Symposium*, 15th-17th March 2005, pp. 187-190. This figure appears as Fig 6 on page 188.]

CHAPTER 2
EXPERIMENTAL FACILITY

Evaporator for Studying Heat Transfer Performance Characteristics

An experimental facility has been fabricated to examine the heat transfer characteristics of different flexible porous membranes with deionized water as the working fluid. The evaporator section consists of a brass block 5 cm X 15 cm and 1cm thick. A slot of 3.8 cm X 12.7 cm and 6 mm deep is machined on the upper side of the block to insert the membrane to be tested (Figure 2-1). Five grooves are machined on the underside of the block. Five type E ungrounded thermocouples are embedded in them using high thermal conductivity paste (Duralco 132). These thermocouples measure the evaporator wall temperature. The evaporator is heated by a Minco flexible electric heater that is placed under the evaporator. This heater simulates a constant heat flux source. It can provide a maximum heat flux of 17 W/cm^2 at 180 volts. The heater area is 50.61 cm^2. Figure 2-2 shows a picture of the experimental facility.

The heater-evaporator assembly is insulated from top and bottom with a flexible foam sandwiched between polycarbonate sheets. Thermocouples are attached to these sheets to note the insulation temperature. The heat loss is calibrated based on the temperature difference between the insulation surface and ambient.

The wicking membrane is placed in the slot and extends into a reservoir. The reservoir is a small water tank (350 cm^3 in volume) made from polycarbonate. A thin brass plate is bolted on to the evaporator block to contain the vapor inside. The evaporator is sealed from all sides to prevent leakage of vapor. At the inlet to the evaporator, sealing is achieved by inserting a thick rubber pad between the membrane and the evaporator lid and sealing it with high temperature Silicone RTV red. The vapor is removed through a copper tube that is soldered to the other end of the evaporator; this tube acts as a vapor line. Evaporator pressure is measured in the vapor

line at a point very close to the evaporator exit. A Validyne DP103-32 pressure transducer, calibrated over a 0-9.5 kPa range is used (Figure A-1).Vapor temperature is measured with a type E grounded thermocouple, inserted in the vapor line. A schematic of the experimental facility is shown in Figure 2-3.

Experimental data is collected using a CIO-EXP 32 multiplexer board and 12-bit DAS-08 A/D card from Measurement Computing Corporation. Since the steady state characteristics of the system are being investigated, the data are collected at frequency of 4Hz and time averaged over a 1 minute period (240 samples). The heater power is varied with a variable auto transformer and voltage and current measurements are taken to determine the power input to the heater.

System for Measurement of Wicking Characteristics

A facility was developed to study the wicking characteristics of porous membranes (Figure 2-4 and 2-5). It comprises of a membrane holder made of polycarbonate sheets. Air is passed from the bottom of the membrane holder. The air flow rate is metered by a ball valve and measured with a rotameter. The rotameter calibration curve, as provided by the manufacturer (Figure A-2 and A-3). A thin screen mesh is attached at the top of the membrane holder to distribute the air flow evenly. The porous membrane is placed over the screen. One end of the membrane is immersed into a reservoir containing water.

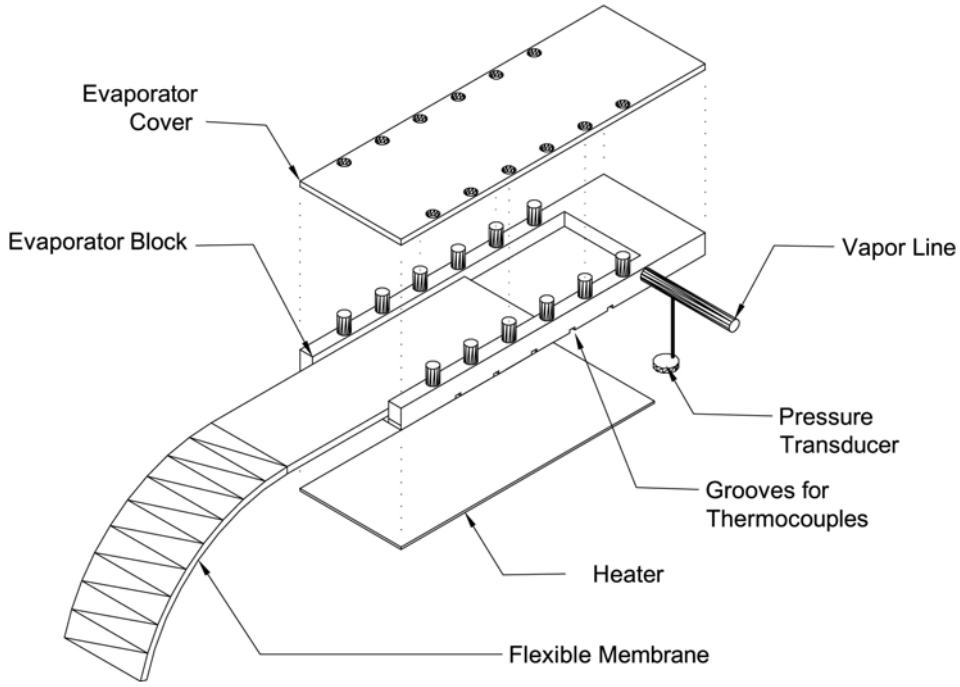

Figure 2-1: Exploded view of evaporator-heater assembly

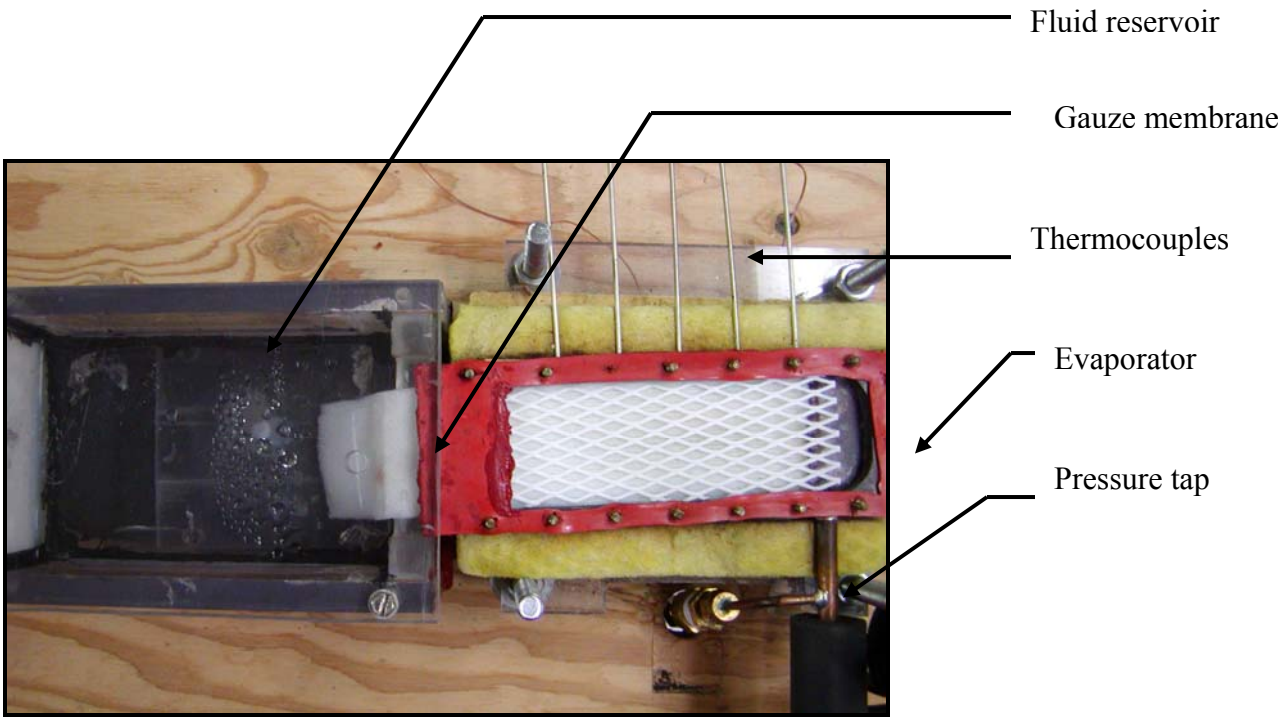

Figure 2-2: Experimental facility for membrane heat transfer characterization

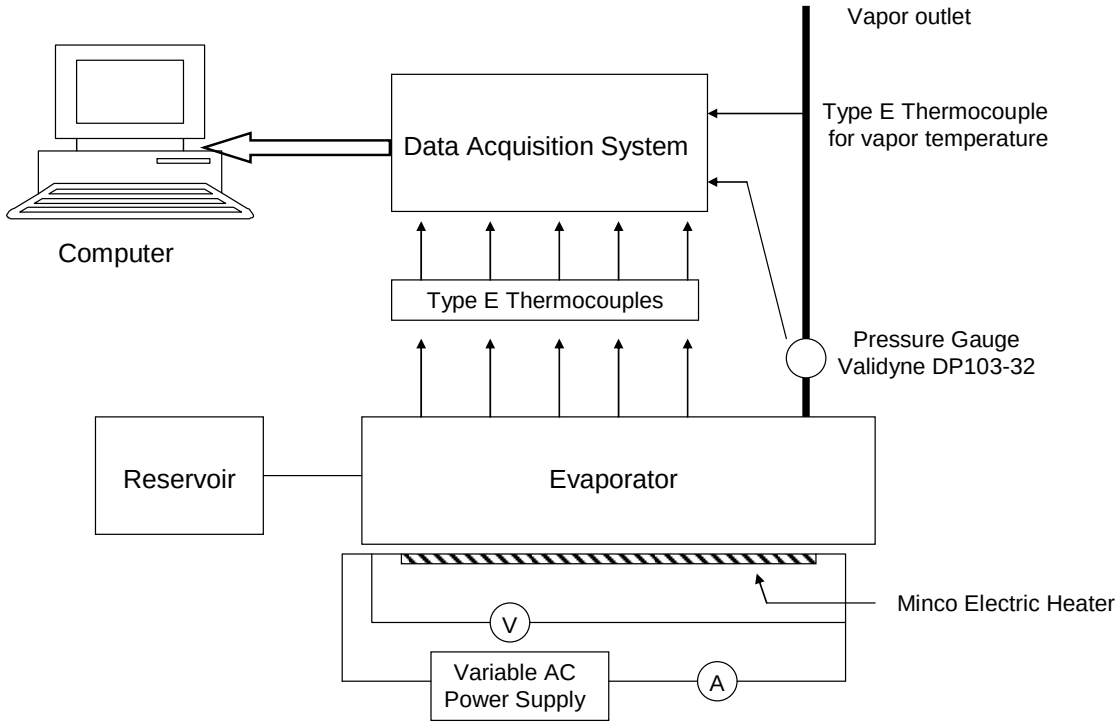

Figure 2-3: Schematic of the experimental facility for studying heat transfer characteristics of membranes.

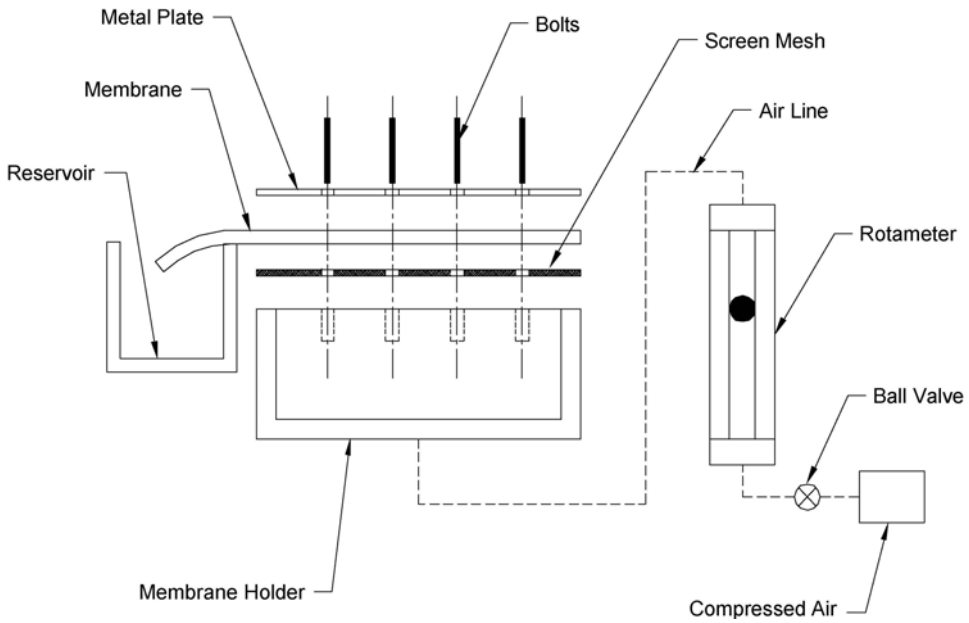

Figure 2-4: Schematic of facility for wicking measurements

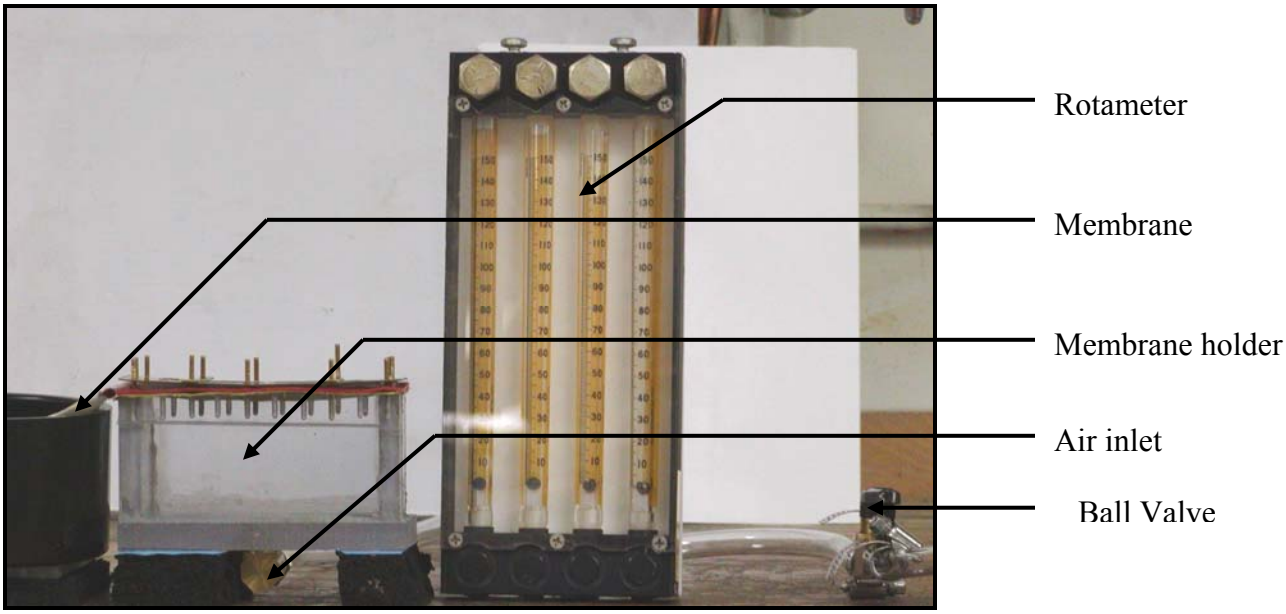

Figure 2-5: Experimental facility for wicking measurements

CHAPTER 3
EXPERIMENTS AND RESULTS

Preliminary Investigation

The heater-evaporator assembly is calibrated for heat loss. This is done by applying low heat loads to an empty evaporator and noting the steady state temperatures of the insulation at each load. As there is no fluid in the evaporator, the heat supplied by the heater is lost to the surroundings at steady state conditions. The heater power is determined by measuring the voltage across the heater and current flowing through it. The power is changed through a variable auto transformer. The heat loss can then be estimated as a function of the difference between the ambient and insulation temperature. A linear relationship is obtained (Figure A-4).

As noted in the literature review, the wicking membrane in the evaporator has a significant influence on the performance of a LHP. In order to design a flexible LHP, it was required to select a flexible membrane and test its performance. Initially 3 different flexible membranes were tested namely—Cellulose membrane, Polyethylene sheets and Blotting paper (Figure 3-1). Their salient features are listed in Table 3-1.

To study the heat transfer characteristics of these membranes, the following experimental procedure is followed. First, the evaporator surface is cleaned and a membrane is placed in the slot. It extends into the fluid reservoir. The evaporator is sealed at all sides. The heat load is applied to the evaporator through the heater and data is collected. When the change in wall and insulation temperatures are within 1^0C over 30 minutes, the steady state is assumed to have been reached and average wall and vapor temperatures are recorded. The heat load on the evaporator is then determined by subtracting the heat loss from the heater power. This procedure is repeated for increasing heat loads until a sudden, sharp rise in wall temperatures is observed, indicating evaporator dryout.

The heat transfer coefficient is computed as the ratio of heat flux to the difference between the average evaporator wall temperature and the saturation temperature. Water is used as the heat transfer fluid for all experiments. Figure 3-2 shows the variation of the heat transfer coefficient with increasing heat flux for the three membranes investigated. The highest heat flux shown is the maximum heat flux possible without reaching dryout. Dryout was assumed when a sudden large rise in observed evaporator wall temperature was observed. It should also be noted that, the temperature profile in the evaporator had a peak near the centre in case of steady state operation but when the input heat flux was increased beyond a certain point, the temperature at the far end of the evaporator increased more rapidly than at other points. At this condition dryout was said to be attained.

The data for polyethylene sheets and blotting paper membrane was curve fitted using the empirical expression given by Eq. 3-1. The values of empirical constants used in Eq. 3-1 are given in Table 3-2.

$$h = A + \frac{B\,\dot{q}''^{k}}{\exp(\dot{q}''^{m}/n)} \qquad (3\text{-}1)$$

For the cellulose membrane, the heat transfer coefficient initially increases and then slightly decreases with further increase in heat flux. A peak heat transfer coefficient is observed. Similar behavior is observed with the blotting paper membrane.The maximum achievable heat transfer coefficient and maximum heat flux before dryout from these tests are listed in Table 3-3.

With regards to the system pressure two different phenomena were observed in these tests. In the case of blotting paper membrane it was seen that the recorded pressure at the evaporator exit increased with an increase in the applied heat load (Figure 3-3).

During these tests the vapor generated in the evaporator was discharged into the ambient. Hence the resistance to flow in the vapor line was very low. The data recorded by the pressure

transducer located at the evaporator exit indicates the frictional pressure drop in the system caused due to the flow of vapor. This pressure drop increases at higher heat flux because more vapor is generated. Hence the system pressure increases with increase in heat flux (Figure 3-3). Kaya and Godak [7] have predicted similar trend from their numerical model for loop heat pipes. They hypothesize that a closed loop heat pipe system can continue operation as long as the pressure required to drive the fluid through the loop is less than the maximum capillary pressure that the wick can sustain. As the heat input to the system increases, the mass flow of vapor increases. Hence the pressure head required at the evaporator outlet increases with increase in heat input.

In the case of Cellulose membrane, a different phenomenon was observed (Figure 3-4). At low heat loads it was seen that the pressure at 'steady –state' had an oscillatory nature. However, the amplitude of these oscillations decreased as the heat load was increased. Figure 3-4 shows the steady state pressure at three different heat loads of 0.22 W/cm2, 0.25 W/cm2 and 0.28 W/cm2 for cellulose membrane. The standard deviations in recorded pressure for the 3 cases are 0.057, 0.021 and 0.023 respectively.

These oscillations point towards an unsteady flow in the vapor line. These observations can be explained with the help of a model developed by Ren et al [11]. They take into account the effects of convection of fluid through the porous membrane (i.e. wicking), heat conduction properties of the membrane and evaporation of fluid in the pores. Pressure fluctuations similar to those described above have been predicted by their model. It is further noted that at low heat fluxes the vapor is 'mostly constrained in some isolated micro-bubbles' [11] in the pores of the wicking membrane. The heat load is insufficient to provide enough energy to drive the vapor in

the vapor line. Hence the vapor flow at low heat flux is intermittent resulting in the observed pressure oscillations.

Wicking Rate Measurements

Following the preliminary tests described above, the wicking rate of the 3 membranes tested was measured. For these tests, membrane samples of size 15 cm x 5 cm are used. The weight of the sample is measured. It is then placed horizontally (with 2.5 cm of its length extended in the reservoir) and one end is lowered in a water reservoir. The time required for the wicking front to reach the other end of the membrane is measured. The membrane is then removed from the reservoir and its final weight is measured. The difference in the final and initial weight and the wicking time measured yield the wicking rate in g/min. This procedure is repeated 3 times for each membrane. For each test, the water in the reservoir is maintained at the same level at the start. The wicking rates of the 3 membranes along with the maximum heat flux reported in 'Preliminary Investigations' earlier are reported in Table 3-4.

From Table 3-4 a direct relation between the wicking rate and the maximum heat flux is observed. In order to yield a higher heat flux it was necessary to find a flexible porous membrane with high wicking rate with water. A number of different types of membranes were tested to estimate their wicking rates (Table 3-5). The procedure followed was exactly same as that described previously for the Cellulose, Blotting paper and Polyethylene sheet membranes. It can be seen that, out of the materials tested, the dressing gauze with 20 layers has the best wicking rate. This material was therefore further investigated to study its heat transfer performance.

Study of Dressing Gauze Performance

It was determined from the wicking tests described earlier that the dressing gauze has a very high wicking rate for water. The thickness of an individual layer is only about 0.125mm. The evaporator slot is 6mm deep. Hence 20 layers of the dressing gauze were stacked together

and used as a wicking membrane in the evaporator for this study. The evaporator-heater set up was used again, and a procedure similar to that described in 'Preliminary Investigations' was followed. The evaporator temperature was measured at 5 locations with the embedded thermocouples. The average evaporator wall temperature corresponding to various values of heat input was calculated. The vapor temperature, measured in the vapor line was found to be constant at 100 ^{0}C. The data obtained is used to plot a boiling curve (Figure 3-5). The heat transfer coefficient is then determined from these data of wall temperatures (Figure 3-6). The maximum heat transfer coefficient obtained was 2864.8 W/m^{2}K and the maximum heat flux before dryout was 5.95 W/cm^2. The test was repeated and the data was seen to be repeatable. The empirical expression fitted to the data in Figure 3-6 is given by Eq. 3-4.

$$h = p_1 x^3 + p_2 x^2 + p_3 x + p_4$$
$$where \quad p_1 = -10.38, p_2 = 79.554, p_3 = 139.35, p_4 = 1413.3 \qquad (3\text{-}2)$$

In order to study the pressure characteristics of this membrane, a ball valve was added to the vapor line of the experimental facility shown in Figure 2-3. The power input to the heater was set to some constant value and the pressure in the system was slowly increased by partially closing the ball valve. Care was taken to ensure that steady state was reached for all values of pressure. It was observed that as pressure in the system was increased, the evaporator wall and insulation temperatures increased slightly and reached a new steady state value. This trend continued till a certain value of system pressure, beyond which the wall temperatures increased very rapidly and dryout was obtained. Figure 3-7 shows this trend for an input heat flux of 2.5 W/cm^2.

It was not feasible to attain steady state at such high temperatures. Hence the exact dryout heat flux and wall temperatures could not be estimated. Hence the immediately preceding value of heat flux is recorded as 'Dryout heat flux' in Figure 3-7. For each value of 'Dryout heat flux',

two values of system pressure have been plotted. The higher value corresponds to observed jump in temperature and the lower value is the pressure value just preceding this reading. Thus for each value of 'Dryout heat flux', the maximum pressure that can be developed in the evaporator lies between the two bands shown in Figure 3-7. This test was repeated for a number of heater power inputs. A relation showing 'dryout heat flux' as a function of 'system pressure' was obtained (Figure 3-7). It can be seen that as system pressure is increased, the dryout occurs at lower heat flux. In other words, the maximum heat transfer capability of the gauze membrane decreases with increasing system pressure.

Effect of Evaporation on Wicking

The wicking rate measurements described earlier were done under ambient conditions and without applying any heat input to the membrane. For the applications in the evaporator of loop heat pipe, the membrane is subjected to heating. When the wicking fluid reaches saturation temperature, evaporation begins to occur. The vapor is formed at the evaporator wall and rises up through the membrane. The presence of vapor bubbles in the membrane is likely to have an effect on the wicking rate. To investigate this phenomenon, pressurized air was blown through the membrane to model the flow of water vapor. The new wicking rates for different values of volumetric air flux rates were measured. The facility developed for wicking measurements (Figure 2-4) was used for this purpose.

The initial weight of the porous membrane to be studied was measured. It was then placed on the screen mesh on the membrane holder. A metal strip was placed around its edges and bolted down on the membrane holder. The flow of air through the membrane was adjusted using a ball valve in the air supply line. A rotameter placed in the same line measured the air flow rate. The air flow was set to a required value and the end of the membrane was lowered in a reservoir containing water. The time required for the water front to reach the other end of the

membrane was measured with stop watch. When the water front reached the other end, the air flow was stopped and the portion of membrane inserted in the liquid was cut off. The membrane was then removed and its final weight was measured. The difference between the two weights and the measured time were used to calculate the wicking rate. This procedure was repeated three times for each air flow setting and average value of wicking rate was determined. Then the air flow rate was set to a different value and the same procedure was repeated. It was observed that wicking flux reduced with increase in volumetric air flux (Figure 3-9).

For the experiments with gauze membrane it should be noted that only 4 layers of gauze were used instead of 20 as in the case of evaporator. Hence, the maximum wicking flux, corresponding to zero airflow, is only 0.041 kg/m^2-s. Further, it was seen from the heat transfer performance experiments that the maximum heat flux before dryout for gauze dressing was approximately 6 W/cm^2. Assuming that all the heat supplied to the evaporator is used for phase change of water, the corresponding maximum vapor volumetric flux will be 0.04386 m^3/m^2-s. As the area of the membrane holder used in air flow experiments is slightly smaller than the evaporator area, the air flow required to attain the same volumetric flux as vapor is 0.017 m^3/m^2-s. So in Figure 3-9, the region of interest is only from 0 to 0.017 m^3/m^2-s on the x-axis. The maximum reduction in wicking rate observed over this range was 5.9%.

As noted earlier, the wicking rate of 20 layers of gauze membrane without applied heat load is 10.36g/min. The water temperature at inlet to evaporator is 25^{0}C and the latent heat of vaporization for water at atmospheric pressure is 2257 kJ/kg. Assuming that the dryout occurs when the rate of vaporization exceeds the rate at which water is replenished to the membrane the maximum heat flux before dryout can be estimated by Eq. 3-3.

$$\dot{q}''_{\max,est} = \dot{m}_{wick}[c_p(T_{sat} - T_{in}) + h_{fg}] \tag{3-3}$$

For the 20 layers of dressing gauze membrane, Eq. 3-2 yields the estimated maximum heat flux to be 7.7 W/cm^2. However, the observed maximum heat flux from the experiments is only 5.95 W/cm^2. This difference is more than 22% and cannot be explained by the reduction in wicking rate due to the presence of vapor flow alone.

It was therefore hypothesized that the wicking rate of the membrane may be different inside the evaporator due to the bolting pressure applied to it and also due to direct contact with Silicone RTV red sealant at the evaporator inlet. So, the wicking rate of the membrane was measured in the actual sealed and bolted evaporator by using the same method as previously described. Two tests were performed and the results are listed in Table 3-6. The average wicking rate from these tests was 4.925 g/min which yields a maximum heat flux of 4.16 W/cm^2 from Eq. 3-3. This results in a 30% lower estimated maximum heat flux value than that observed in experiments.

Effect of Length on Wicking

All the results reported in the previous sections, for various membranes pertain to membrane and evaporator length of 15.4 cm. It was observed that wicking rate inversely proportional to the total length of the membrane. Wicking rate measurements, as described in section 'Wicking Rate Measurements' were carried out for different lengths of the wicking membrane. The membrane used was 4 layers of dressing gauze. The results (Figure 3-10) can be explained by Washburn's equation [26], given as Eq. 3-4, which is applicable for homogeneous porous media and low fluid velocities.

$$u = \frac{K\sigma_l \cos\theta}{4\mu x} \tag{3-4}$$

In Eq. 3-4, θ is the contact angle of liquid with the membrane, σ_l is the liquid surface tension and x is the length of the wicking membrane.

The wicking rate can be increased by up to 80% by a 50% reduction in the evaporator length (Figure 3-10). The resulting predicted increase in dryout heat flux is about 250%. It should be noted however that the effects of reduction in wicking rate due to bolting pressure and sealing in the actual evaporator are ignored in this analysis.

Study of Complete Loop Heat Pipe System

The results reported in earlier sections pertain only to the evaporator of the loop heat pipe. In order to study the complete loop heat pipe system, a condenser was connected to the vapor line. The condensate from the condenser was returned to the fluid reservoir (Figure 3-11). The cooling water for the condenser was provided by a laboratory chiller (not shown in the figure).

However two main problems were encountered in operating this system. First of all, due to the presence of non condensable gases in the water, the condensation heat transfer process in the condenser was inefficient. Hence vapor could not be completely condensed in the condenser. Secondly, this uncondensed vapor in the condenser resulted in back pressure on the evaporator. As discussed in earlier sections, the evaporator performance deteriorates in the presence of back pressure (see Figure 3-7 and 3-8). Hence higher wall temperatures were observed at moderate to low heat fluxes. Due to the risk of overheating the Mica heater, the heat flux could not be increased close to the dryout heat flux value.

As the focus of the present study is to develop and demonstrate the operation of a flexible evaporator, the condenser problem is not resolved at this point. However it is recommended to have degassing system in the condenser and design a more efficient condenser for future work.

Design and Performance of Flexible Encasing

In order to develop a flexible evaporator, a flexible encasing is required for the membrane. This encasing needs to be deformable so that it can adapt to the shape of the heat source. The phase change will take place within this encasing. This encasing is referred to as flexible

evaporator. For this purpose, the 'flexible barrier pouches' manufactured by Tolas Inc. were used. The material of these pouches is 104 micron thick and consists of laminates of aluminum and polyethylene. The membrane is inserted in the pouch with 1" of membrane extending out from the pouch into the reservoir. The membrane is pressed down by using 8 cylindrical viton rubber inserts of 3 mm diameter and 6 mm length each. A flexible tube of 6.3 mm diameter is inserted at the other end. The pouch is then heat sealed from all the sides using a heat sealer. The gap between the membrane and pouch material is sealed using a rubber pad insert and Silicone RTV Red glue. Three thermocouples are attached to the underside of the pouch on the outer wall. This assembly (Figure 3-12) is placed on a heater and insulated from all sides. The heater used for this set of experiments is a 120V, 240 W, rectangular heater of surface area 43.5 cm^2. The heater-insulator assembly is insulated with fiber glass insulation and foam insulation from top and bottom. The insulation is pressed between two polycarbonate sheets and the entire assembly is held together by four bolts. This system is calibrated for heat loss (Figure A-5).

To test the heat transfer performance of this flexible evaporator, the membrane is inserted in the reservoir containing water and the evaporator is subjected to different heat flux levels. The steady state temperatures of the evaporator surface and the insulation are noted for each heat flux level. The wall superheat and heat transfer coefficient are obtained based on the measured values (Figures 3-13 and 3-14). The maximum heat flux observed was 3.2 W/cm2 and maximum heat transfer coefficient of 1165 W/m2K was obtained. It should be noted that the heat flux was limited by the heater-insulation assembly and dryout was not observed in these tests.

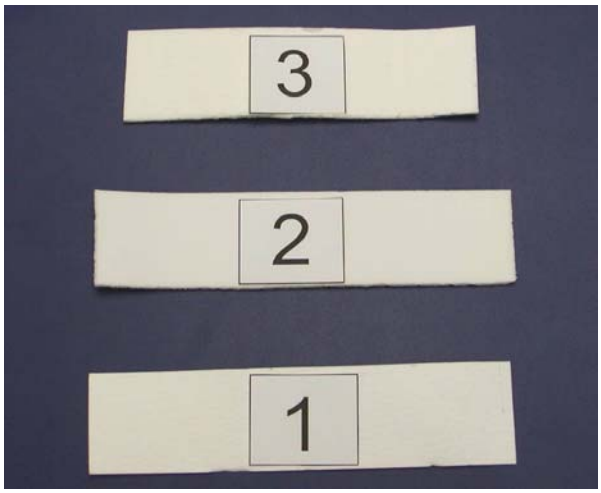

Figure 3-1: Pictorial view of membranes tested: Cellulose (1), Polyethylene sheets (2) and Blotting paper (3)

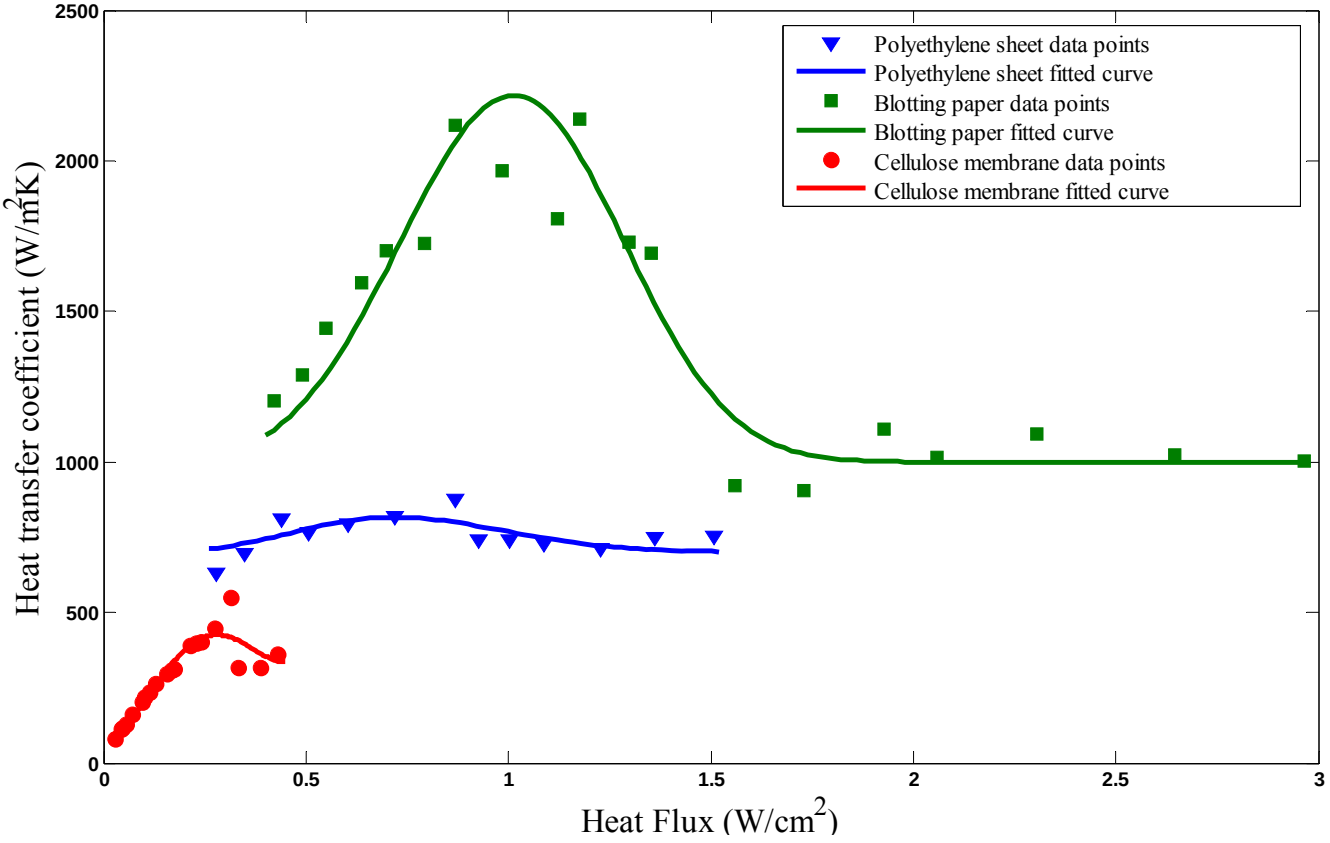

Figure 3-2: Heat transfer characteristics of the 3 membranes tested

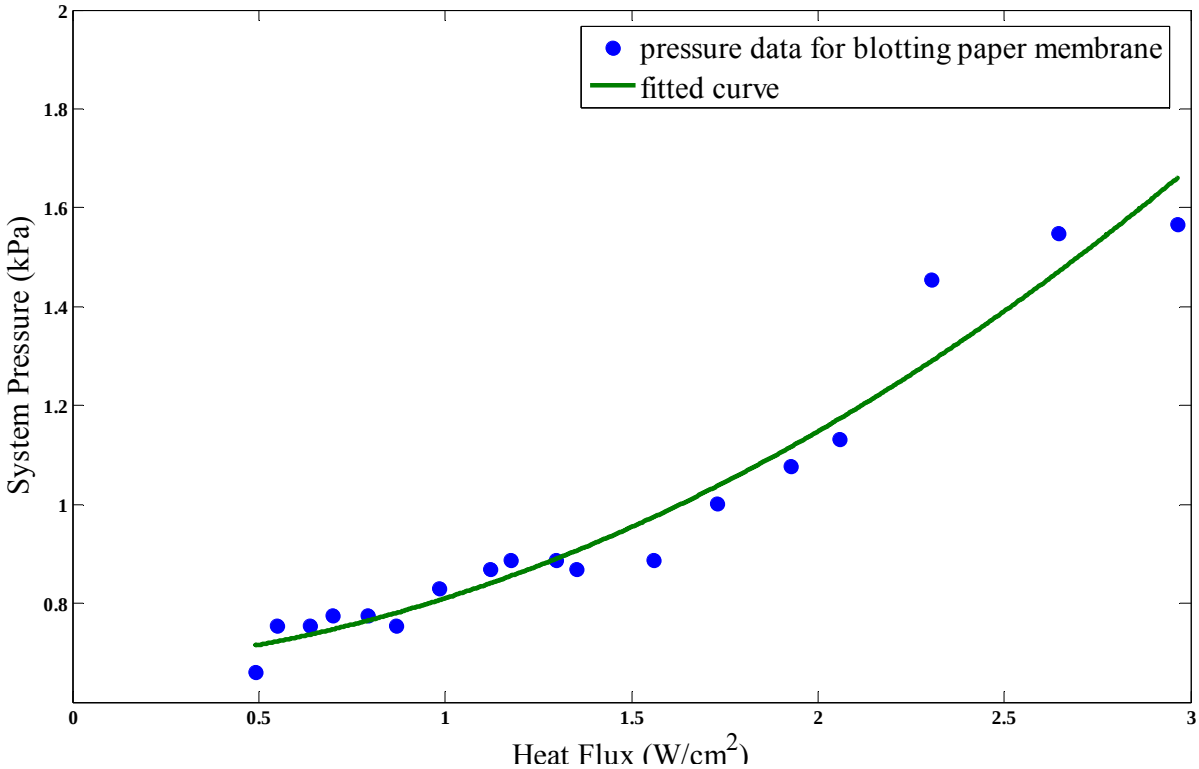

Figure 3-3: Pressure characteristics of the Blotting Paper membrane

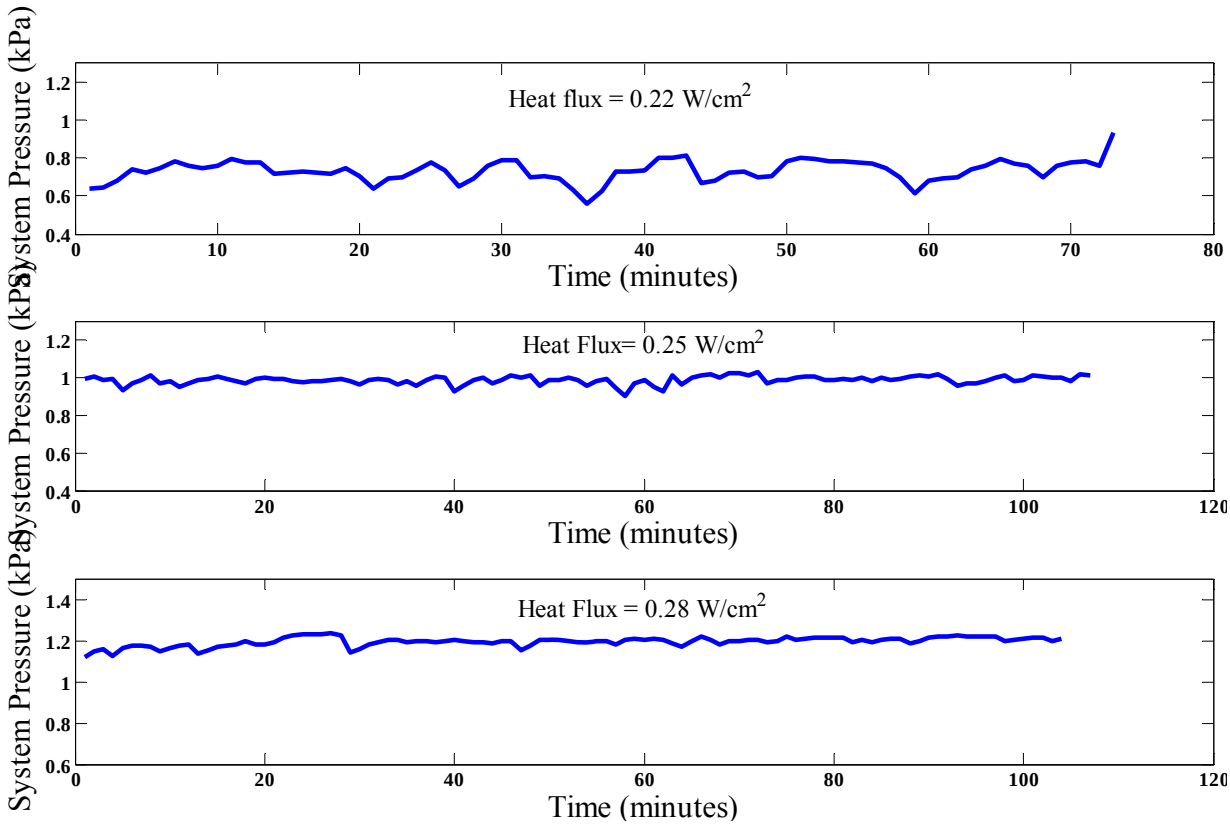

Figure 3-4: Pressure oscillations under various heat loads for cellulose membrane

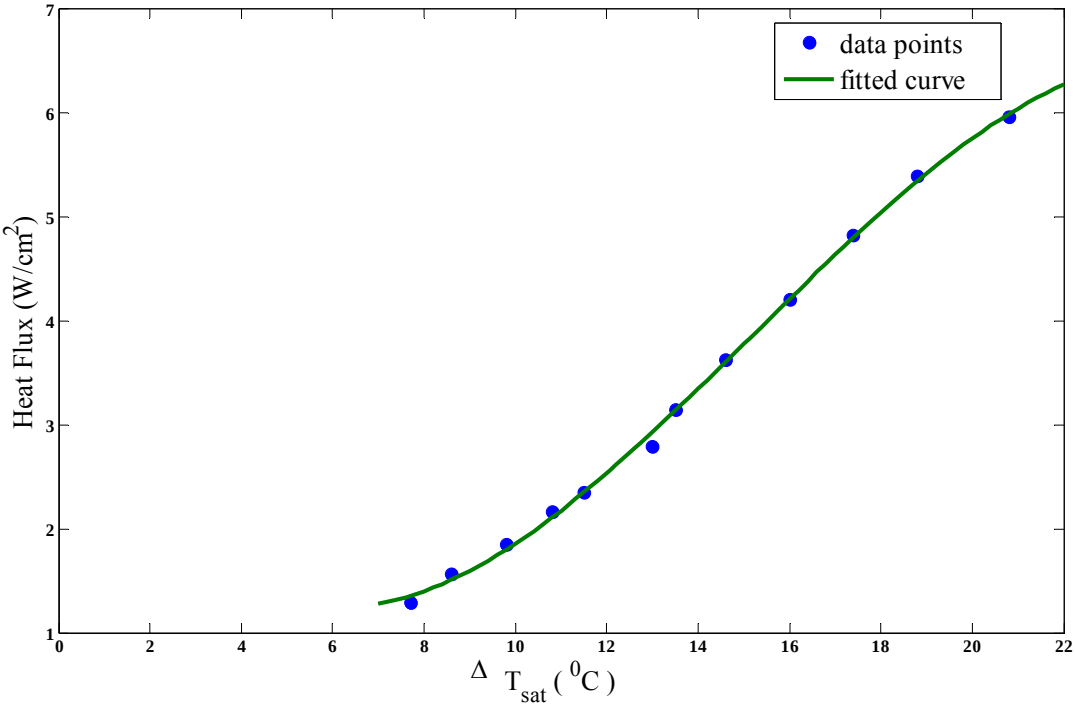

Figure 3-5: Wall superheat for evaporator using dressing gauze membrane

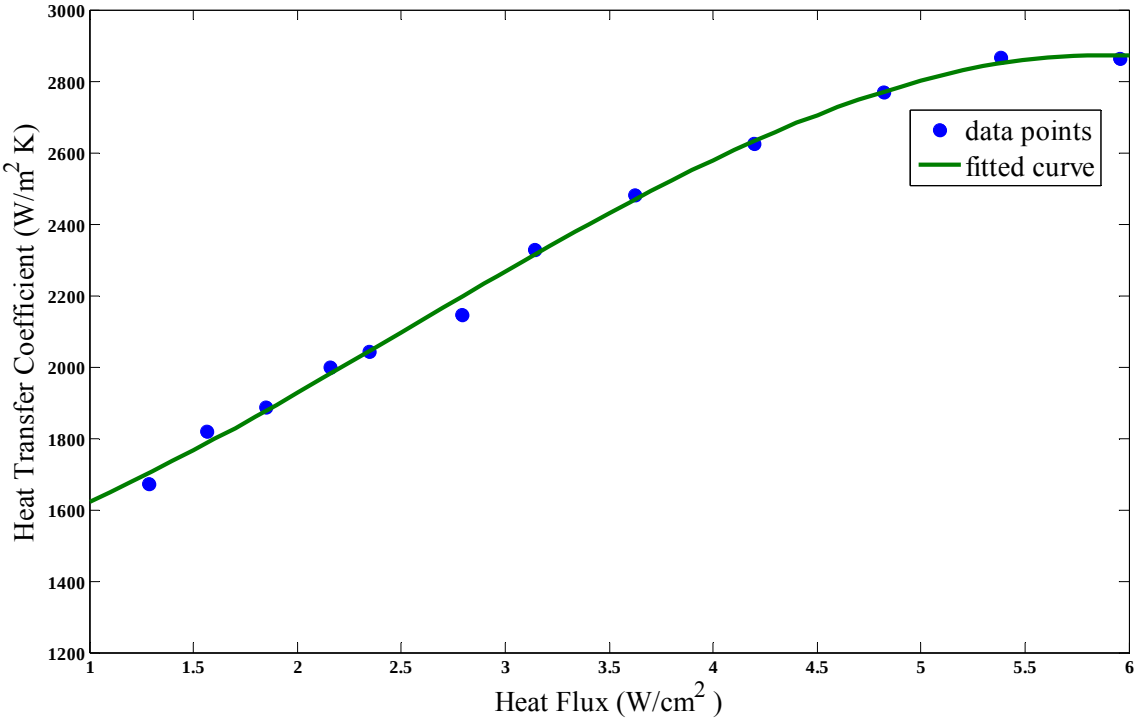

Figure 3-6: Heat transfer performance of dressing gauze as wicking membrane

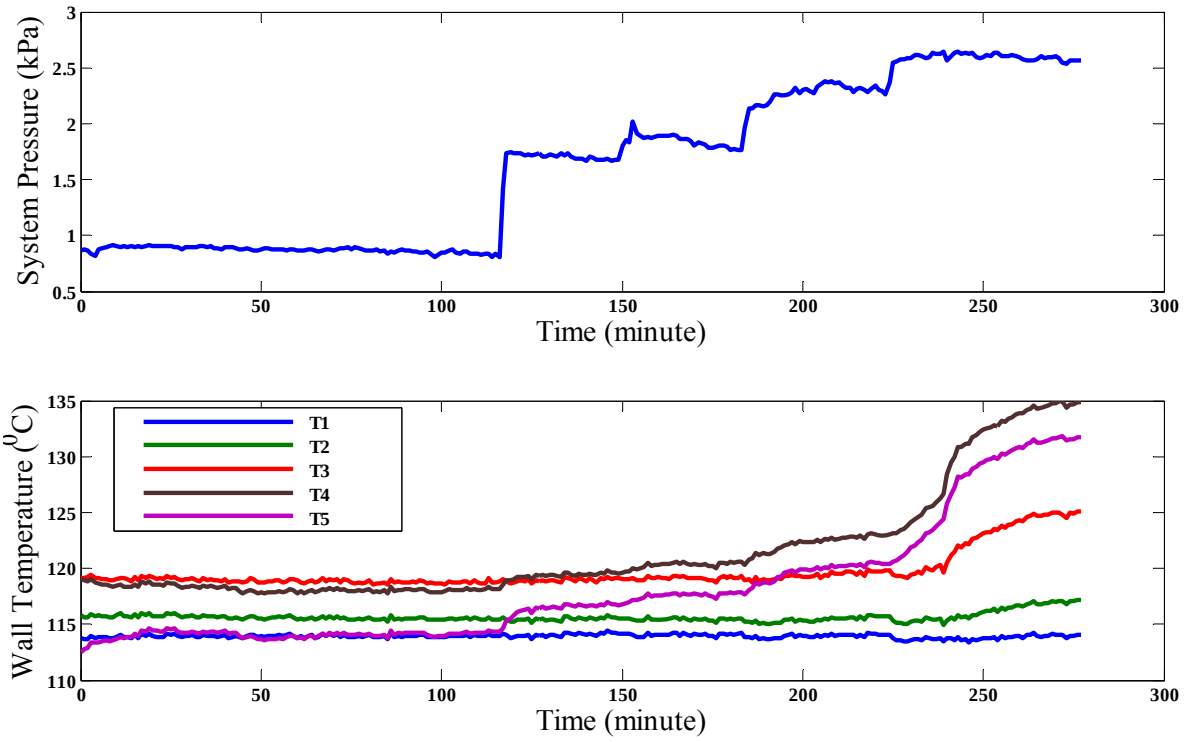

Figure 3-7: Response of wall temperatures to the increase in system pressure for input hear flux of 2.5 W/cm^2.

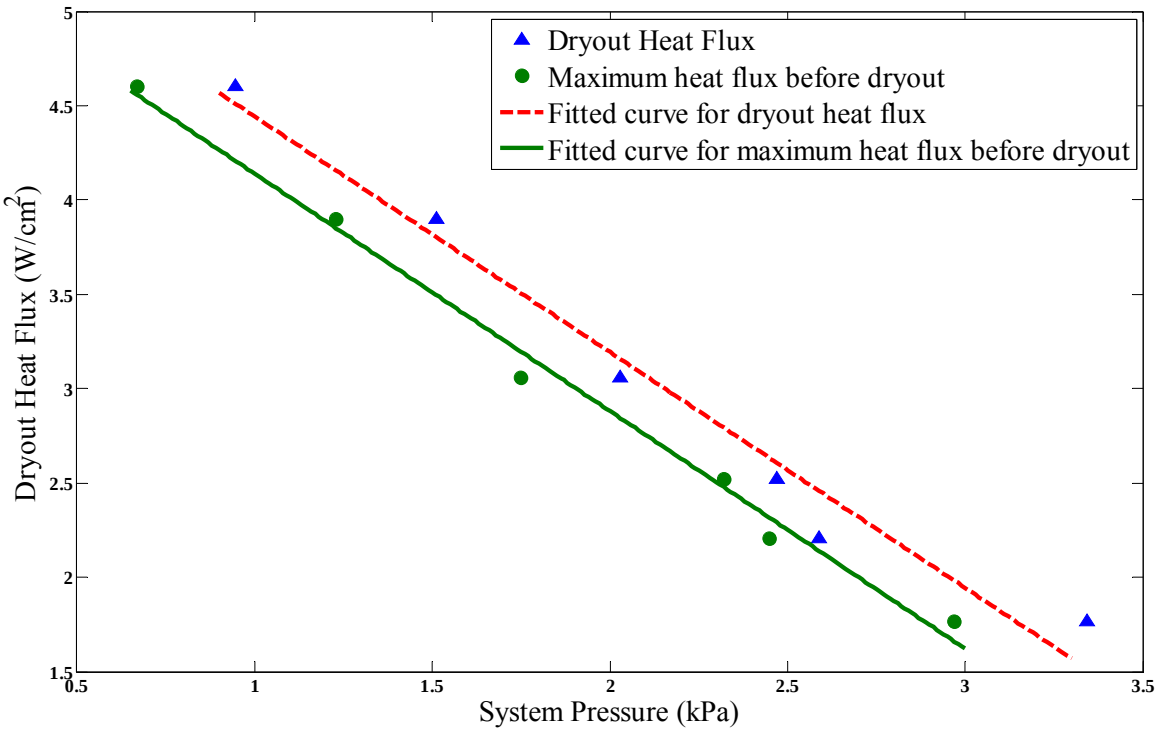

Figure 3-8: Maximum heat flux as a function of system pressure drop for dressing gauze

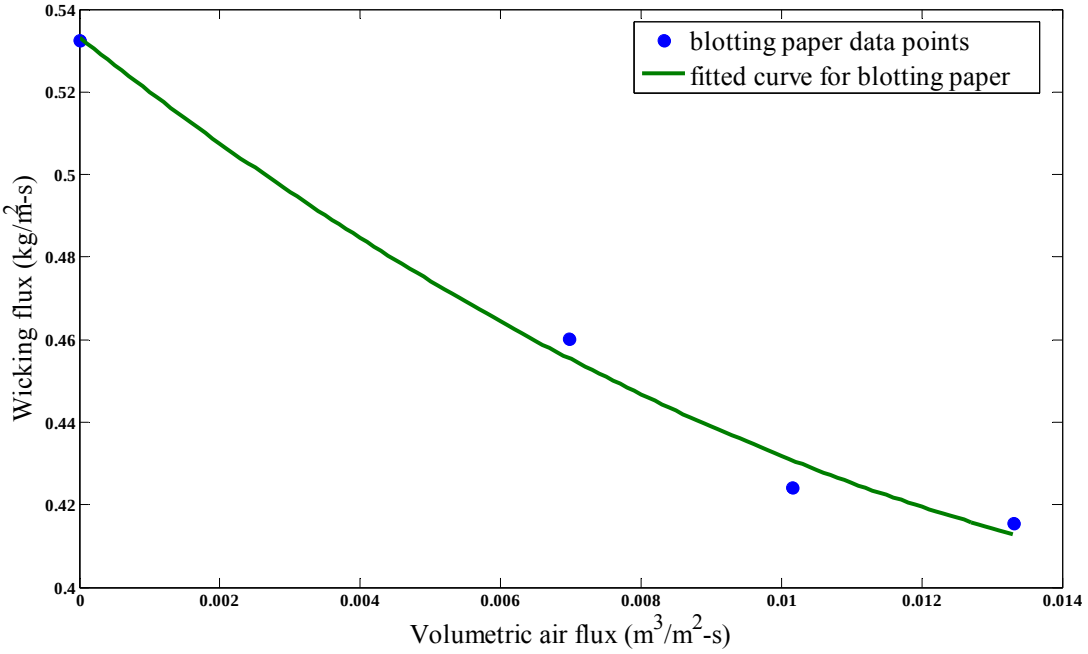

A

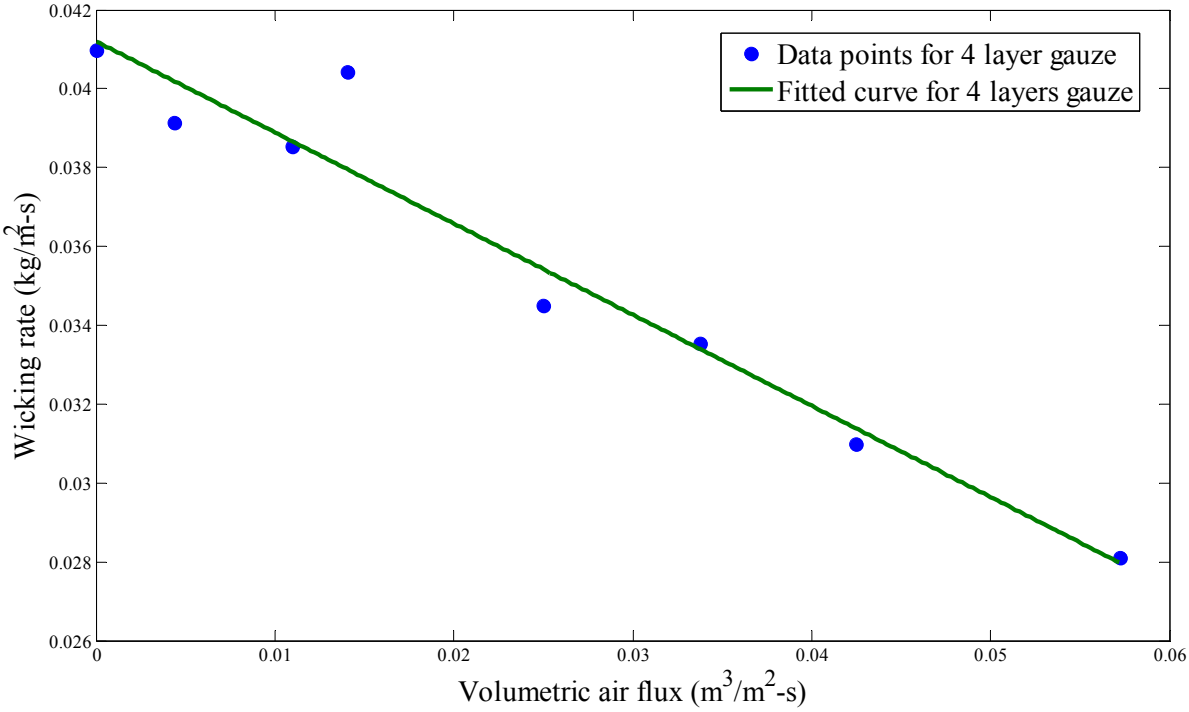

B

Figure 3-9: Effect of air flow on wicking rate. A) Blotting paper membrane B) Gauze membrane

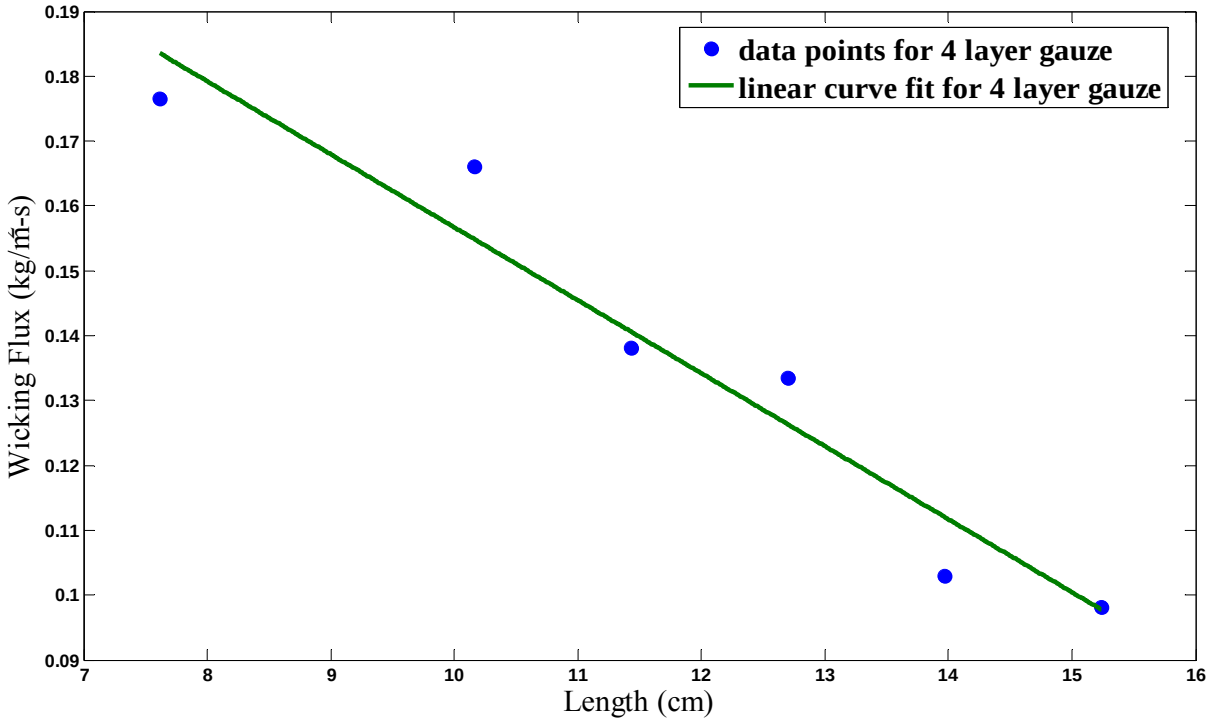

Figure 3-10: Effect of length of membrane on the wicking flux

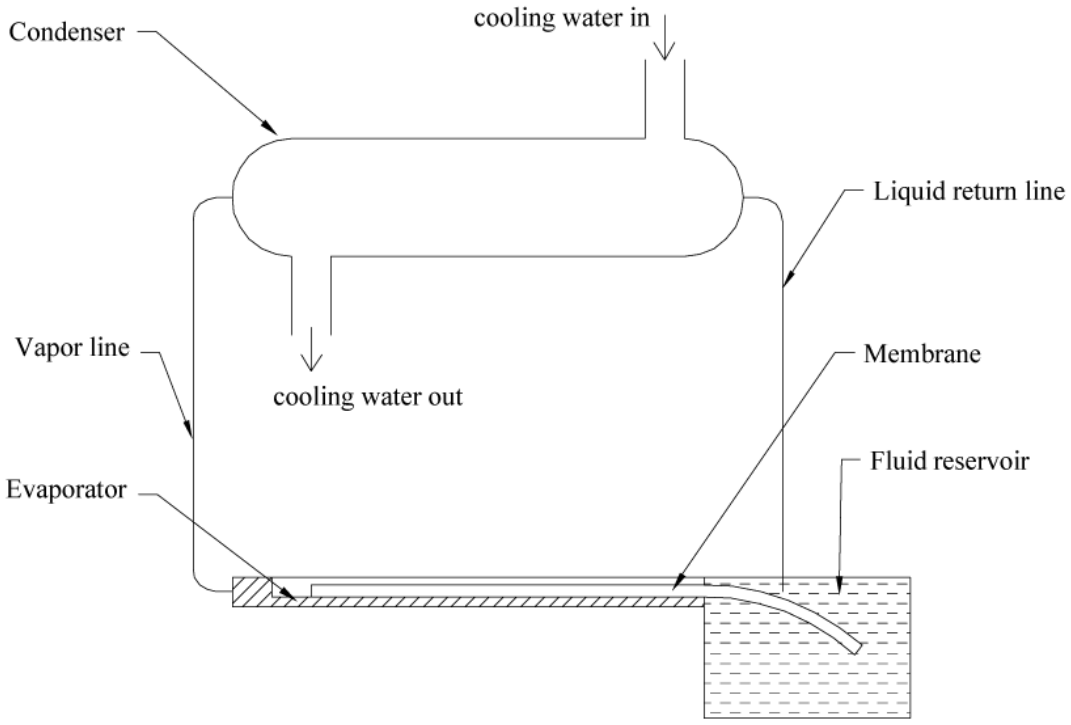

Figure 3-11: Schematic of loop heat pipe system including the condenser

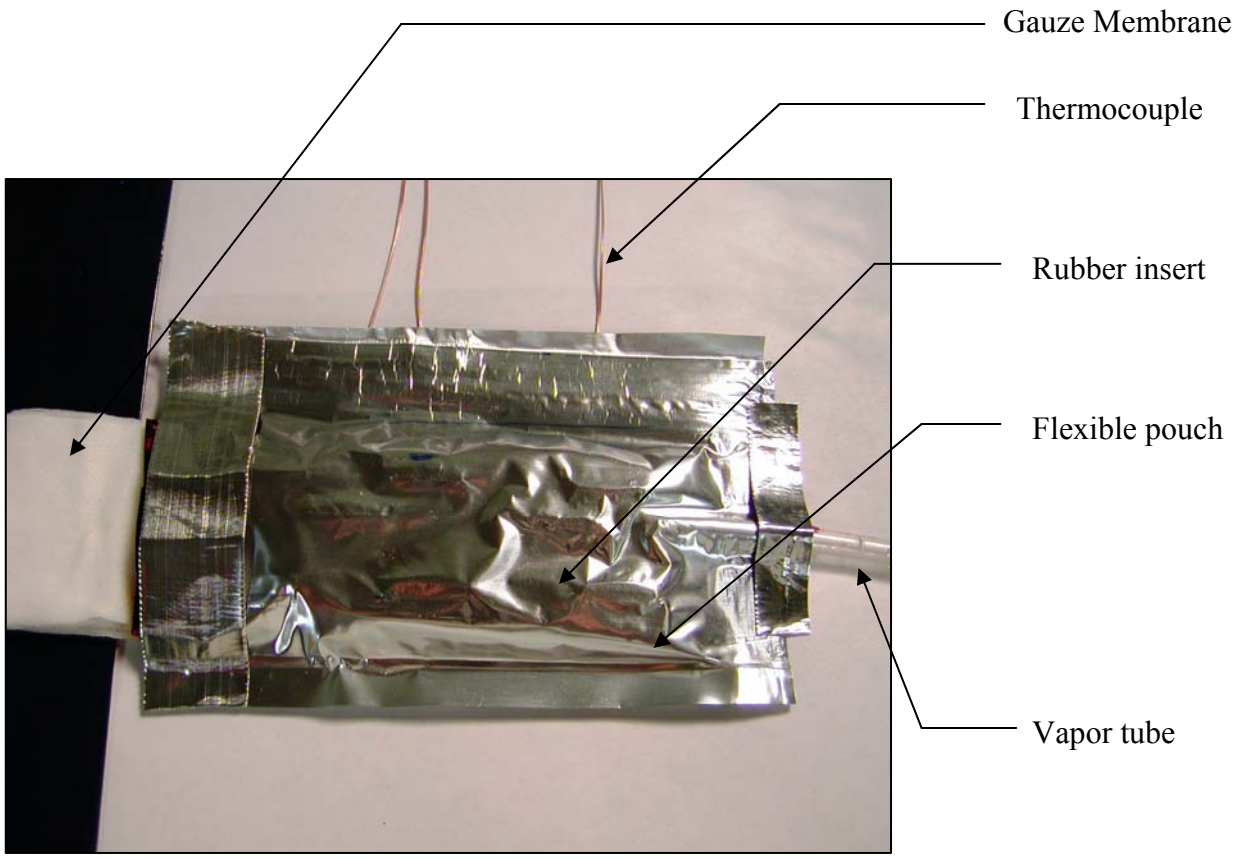

Figure 3-12: Flexible evaporator assembly

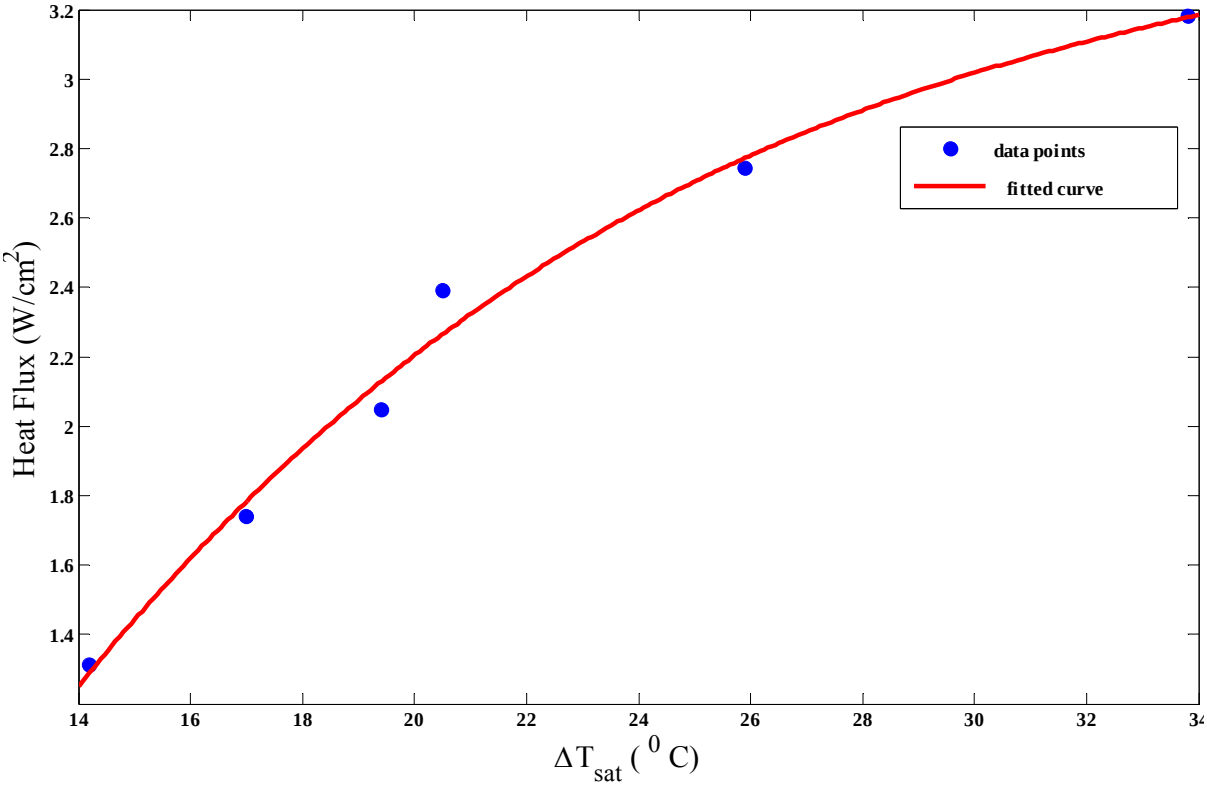

Figure 3-13: Wall superheat for flexible evaporator using dressing gauze membrane

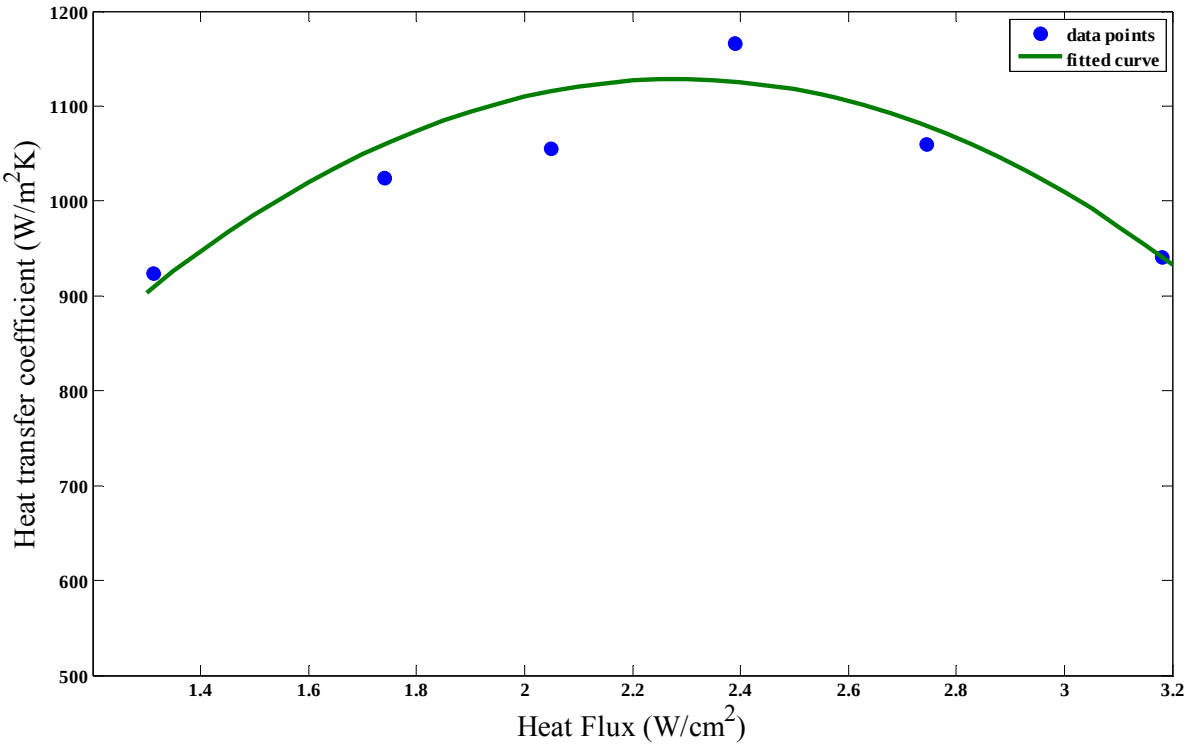

Figure 3-14: Heat transfer performance of flexible evaporator using dressing gauze as wicking membrane.

Table 3-1: Characteristics of the membranes tested

Membrane type	Manufacturer	Thickness (mm)	Pore Size (micron)
Cellulose	Millipore	0.8	89
Polyethylene sheets	Porex	3	110
Blotting paper	Invitrogen	2.5	81

Table 3-2: Values of empirical constants used in Equation 3-1

	A	B	k	m	n
Polyethylene sheet	700	3200	4	2	0.26
Blotting paper	1000	4000	4.1	3.3	0.84

Table 3-3: Results of preliminary investigations

Membrane	Maximum heat transfer coefficient W/m^2K	Maximum heat flux before dryout W/cm^2
Cellulose membrane	551.3	0.43
Polyethylene Sheet	876	1.5
Blotting paper	2100	2.9

Table 3-4: Measured wicking rate of the 3 membranes

Membrane type	Wicking rate (g/min)	Maximum heat flux before dryout (W/cm^2)
Cellulose	0.4	0.43
Polyethylene sheets	2.07	1.5
Blotting paper	4.5	2.9

Table 3-5: Wicking rates for various materials tested.

Product	Wicking rate (g/min)	Membrane Thickness (mm)	Comments	Manufacturer	Wicking flux (kg/m^2-s)
Butler Dustall	N/A	0.15	No wicking observed even after 2 minutes	Butler Home Products Inc	N/A
Kitchen Wipes	1.340	0.5		Cadie Products Corporation	1.172
CHR (Chromatography) grade paper	N/A	0.3	Wicks up to 5 cm -8 cm length only	Whatman	N/A
GB005 membrane	1.383	1.25		Whatman	0.4838
Epage blotting paper	1.016	0.8		Invitrogen	0.6351
Polyester felt	5.901	3		Sutherland Felt Company	0.8604
Absorbent pad	6.670	—	Disintegrated without completely wicking after 8 minutes	Kimberley Clarke Corporation	N/A
Metallic felt	0.218	0.8		Technetics Corporation	0.1191
Cotton fiber membrane	-	-	Very slow wicking	Alhstom	N/A
522A Blotting paper		0.28	Very slow wicking	V&P Scientific, Inc.	N/A
Dressing gauze (20 layers)	10.36	1.1-1.2	Rapid wicking observed	CVS Pharmacy	5.1011
Surgical pad	3.393	0.7		Johnson & Johnson	1.1615
540DB1 (11.5 cm X 3.8 cm sample) membrane	1.760	0.45	non-uniform wetting	V&P Scientific, Inc.	1.710

Table 3-6: Data from wicking rate measurements in sealed and bolted evaporator

Reading Number	Initial Weight (g)	Final Weight (g)	Time (s)	Wicking rate (g/min)	Wicking Flux (kg/m^2-s)
1	2.9	17	163.53	5	0.0143
2	3.7	19.2	191.87	4.85	0.0139

CHAPTER 4
SUMMARY OF RESULTS

The design of a flexible loop heat pipe is significantly different from that of a conventional loop heat pipe. First, the liquid supply line or secondary wick from the compensation chamber to the evaporator is eliminated as it can lend rigidity to the system. Secondly, the evaporator section is made flat instead of tubular. This has two advantages. It makes it possible for the evaporator to conform to the shape of the heat source. Further, any type of saddle or connection from the flat heat source to the evaporator (tubular) is eliminated, thus reducing the contact resistance between the heat source and evaporator.

In the absence of a liquid supply line and secondary wick, the primary wick is responsible for ensuring adequate liquid supply to the evaporator section. Hence the wick is selected based on its flexibility and wicking rate. Conventional loop heat pipes use wicks with as small a pore radius as possible because it results in higher capillary pumping pressure. However, in this study it was observed that the wicks having larger pore size have higher permeability due to reduced flow resistance. Such wicks have greater wicking rates and hence are more suitable for a flexible prototype. In addition, the grooved structure typically employed in LHP evaporators to remove vapor has not been used here. Such a structure will also lend rigidity to the evaporator.

The changes in design mentioned above have been observed to have an impact on the basic principle of operation of this flexible prototype. The maximum heat flux that can be transported through this system depends on the wicking rate of the flexible membrane employed. In typical LHPs, the maximum capillary pressure that can be developed in the wick limits the maximum heat flux. The mechanism of heat transfer observed in this system is boiling. The pumping power for this system is obtained not by the capillary pressure but by the pressure exerted by vapor constrained in the small space of the evaporator. The rate of vapor formation increases as more

and more heat is transferred to the evaporator. The presence of vapor in the wick reduces the wicking rate. This results in the actual heat flux limit being lower than that predicted. Also, the vapor bubbles formed at the heated evaporator wall have to rise through the membrane (wick) to enter the vapor space. As the rate of bubble formation increases, the contact between the wick and evaporator wall may become poorer, resulting in high wall temperature and hence lower heat transfer coefficients.

Another important parameter affecting the performance of this system is the length of evaporator. It was observed that the wicking rate for the membrane was inversely proportional to the length of the membrane. All the results from this study pertain to a fixed total membrane length of 15 cm. However, wicking tests carried out on 11 cm long gauze membrane have shown 40-50% faster wicking rates. This indicates a potential to transfer up to 50% higher heat flux although the total heat transferred may reduce.

Significant improvements to the current results can be obtained by reducing the active length of the evaporator and using better techniques to improve the contact between the membrane and evaporator wall. In all the designs it is necessary to ensure that the vapor removal from the evaporator is efficient at all times.

APPENDIX A
CALIBRATION CURVES

Calibration of Pressure Transducer

The pressure transducer used in this study, Validyne DP103-32 was calibrated from 0 to 9.5 kPa with a wall barometer. The fluid used was barometric oil of specific gravity 0.827.

Calibration Curve for Rotameter

a. N034 tube: The calibration curve (Figure A-2) was provided by the manufacturer of Rotameter, Cole-Parmer. This calibration is performed for N034 tube having a glass float. The range of air flow rate measurement for this tube is 0 to 8678 ml/min.

b. N044 tube: The calibration curve (Figure A-3) was provided by the manufacturer of Rotameter, Cole-Parmer. This calibration is performed for N044 tube having a glass float. The range of air flow rate measurement for this tube is 0 to 23742 ml/min.

Calibration Curve for Heat Loss

The heater evaporator assembly was calibrated for heat loss as described in chapter 2. Figure A-4 shows the heat loss calibration curve for the Minco heater-brass evaporator assembly. Similar calibration curve was obtained for the flexible evaporator set up (Figure A-5).

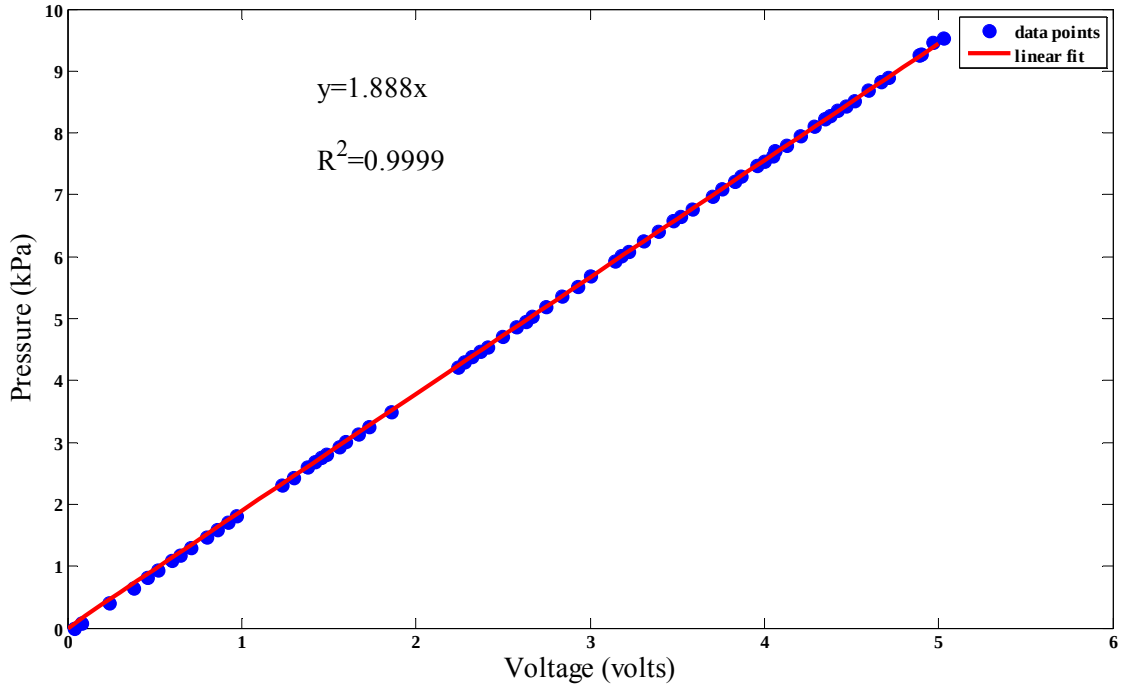

Figure A-1: Pressure transducer calibration curve

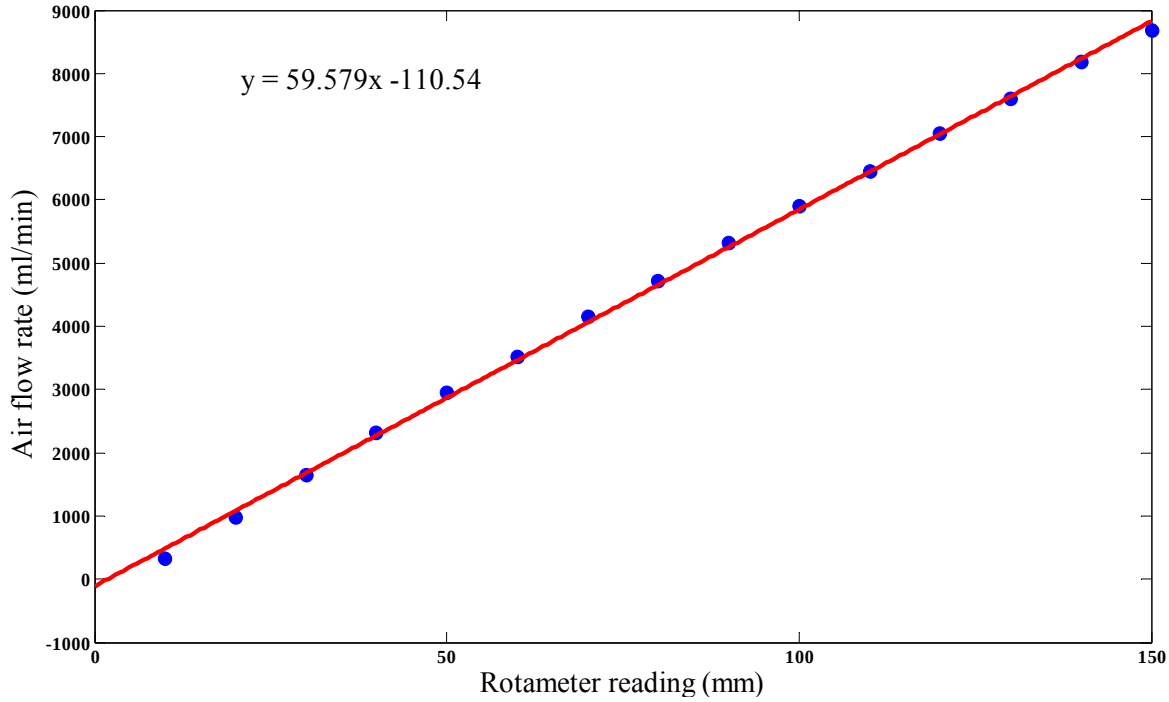

Figure A-2: Calibration curve for Rotameter tube N034

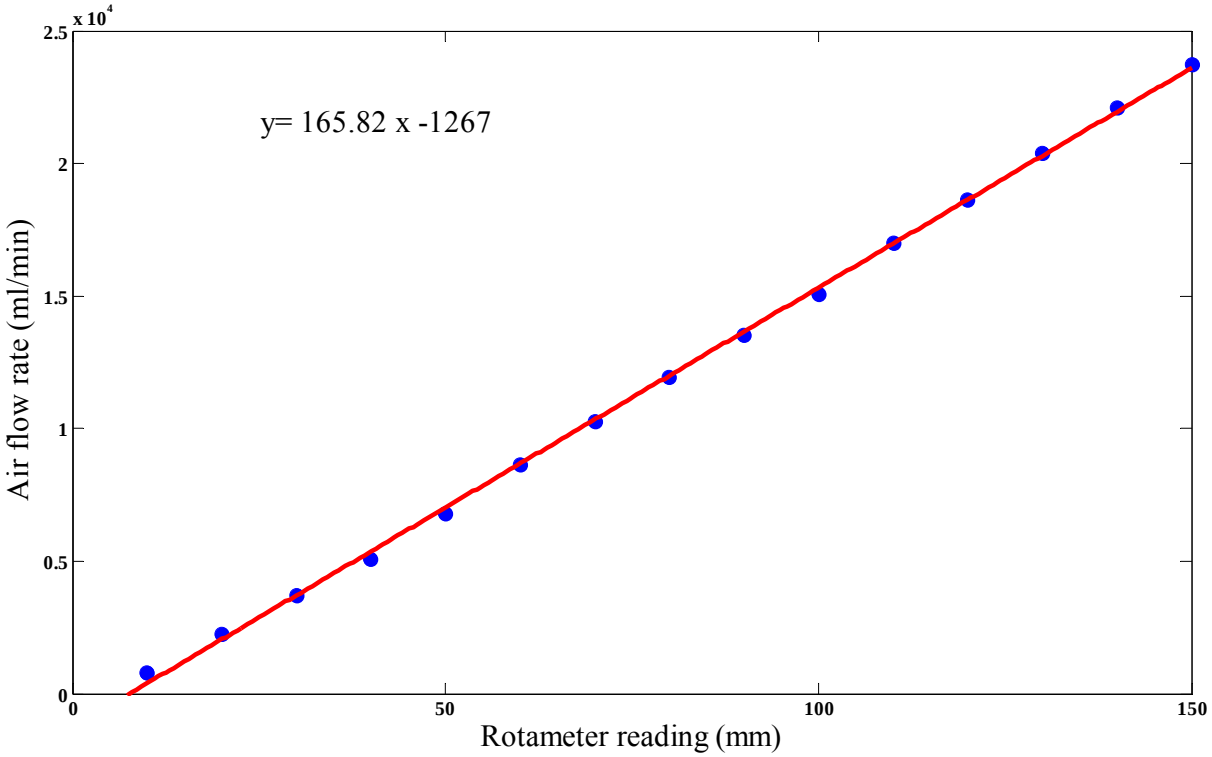

Figure A-3: Calibration curve for Rotameter tube N044

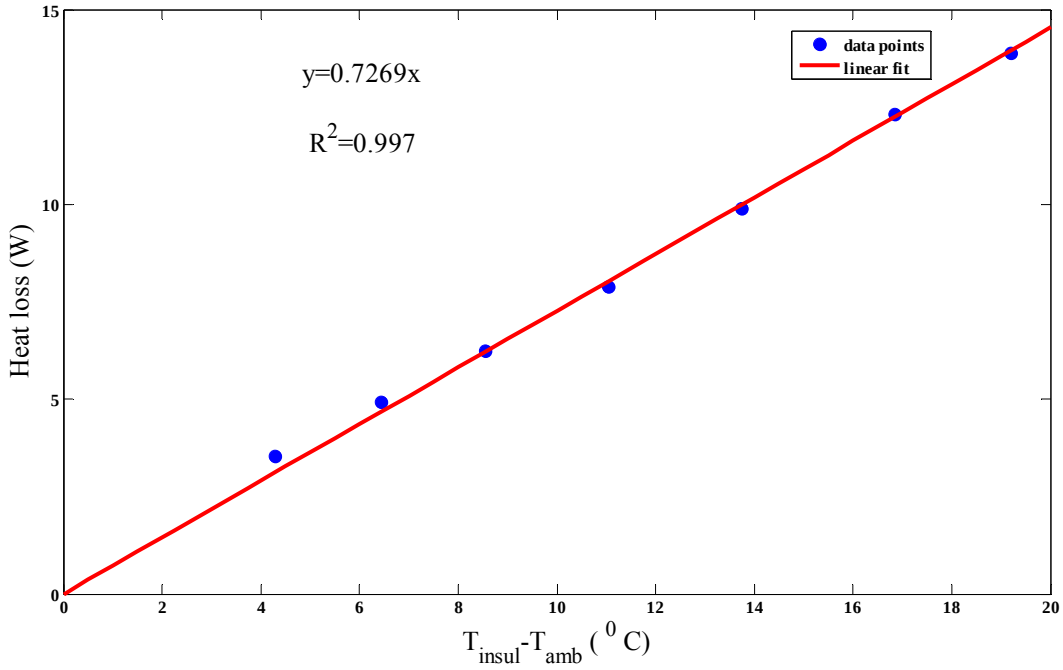

Figure A-4: Calibration curve for heat loss for the heater-brass evaporator assembly.

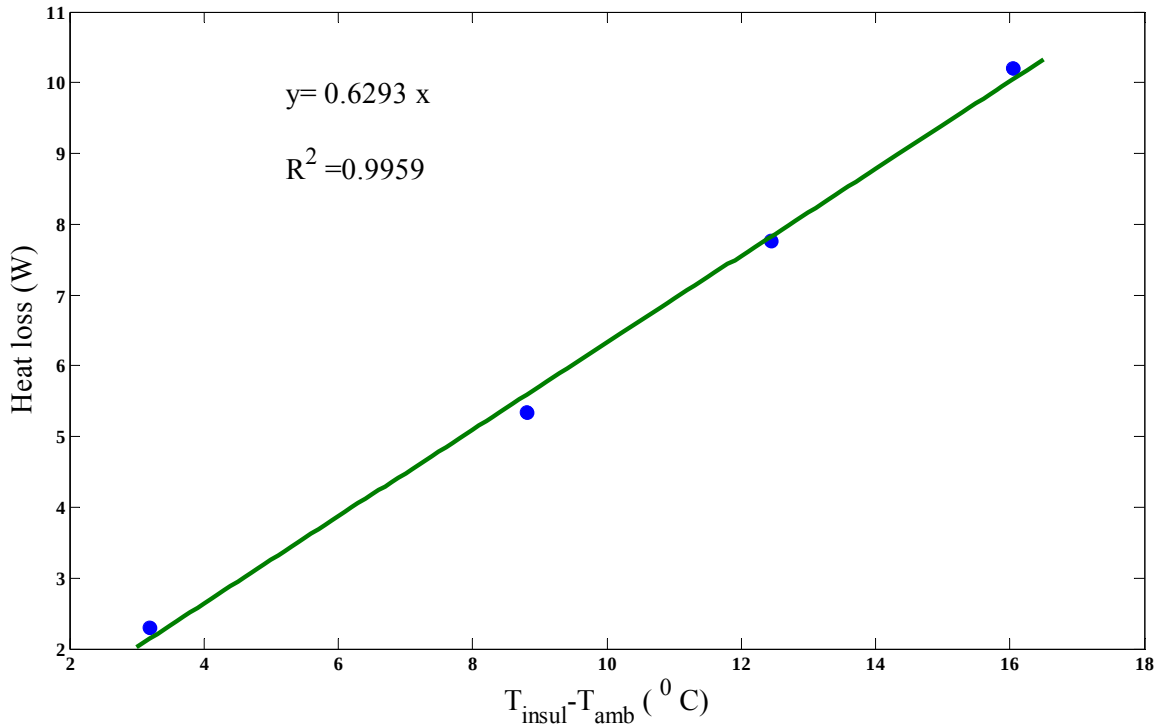

Figure A-5: Calibration curve for heat loss for the heater-flexible pouch evaporator assembly.

APPENDIX B
MEASURED DATA

Table B-1: Measured data and calculations for heat transfer characteristics of dressing gauze membrane in the brass evaporator-heater assembly

Voltage (volt)	Current (ampere)	Average evaporator temperature (^{0}C)	Average insulation temperature (^{0}C)	Ambient air temperature (^{0}C)	Heat flux[a] (W/cm^2)	Heat transfer coefficient (W/m^{2}K)
45.3	1.70	107.7	41.0	24.7	1.286805	1671.175
49	1.84	108.6	40.7	25.7	1.565306	1820.124
53	1.98	109.8	41.5	25.8	1.848008	1885.722
57.1	2.13	110.8	42.2	25.2	2.158975	1999.05
60.1	2.24	111.5	47.8	26.1	2.348355	2042.048
65.4	2.42	113.0	49.5	26.1	2.790401	2146.462
69.8	2.54	113.5	51.0	25.9	3.142597	2327.849
74.8	2.71	114.6	52.5	25.8	3.621809	2480.691
80.5	2.90	116.0	54.1	25.3	4.199077	2624.423
86.3	3.09	117.4	57.2	25.9	4.819503	2769.829
91.6	3.24	118.8	59.2	25.9	5.385857	2864.818
95.9	3.41	120.8	60.9	25.8	5.956698	2863.797

a- Surface are of heater is 51.61 cm^2

Table B-2: Measured data and calculations for heat transfer characteristics of dressing gauze membrane in the flexible pouch evaporator

Voltage (volt)	Current (ampere)	Average evaporator temperature (^{0}C)	Average insulation temperature (^{0}C)	Ambient air temperature (^{0}C)	Heat flux[b] (W/cm^2)	Heat transfer coefficient (W/m^{2}K)
65.9	1.106	114.2	50.6	25.6	1.31235132	924.191071
74.4	1.26	117	54.4	25.9	1.740733639	1023.96096
80.8	1.35	119.4	57.5	25.9	2.048085419	1055.71413
85.5	1.436	120.5	55.7	26	2.390075545	1165.89051
93.5	1.525	125.9	62.7	26.1	2.745238117	1059.9375
99.9	1.66	133.8	69.8	26.4	3.180766475	941.05517

b- Surface are of heater is 43.55 cm^2

LIST OF REFERENCES

1. Grover, G.M., Cotter, T.P., and Erickson, G.F., "Structures of Very High Thermal Conductance," *Journal of Applied Physics*, Vol. 35, No.6, 1964, pp. 1990-1991.

2. Silverstein, C., *Design and Technology of Heat Pipes for Cooling and Heat Exchange*, Hemisphere Publishing Corporation, Washington DC, 1992.

3. Riehl, R., and Siqueira, T., "Heat Transport Capability and Compensation Chamber Influence on Loop Heat Pipe Performance," *Applied Thermal Engineering*, Vol. 26, 2006, pp. 1158-1168.

4. Maydanik, Y., "Review: Loop Heat Pipes," *Applied Thermal Engineering*, Vol. 25, 2005 pp. 635-657.

5. Cheung, K., Hoang, T., Ku, J., and Kaya, T., "Thermal Performance and Operational Characteristics of Loop Heat Pipe (NRL LHP)," *International Conference on Environmental Systems*, Society of Automotive Engineers, Danvers, 1998.

6. Kaya, T., and Hoang, T., "Mathematical Modeling of Loop Heat Pipes and Experimental Validation," *Journal of Thermophysics and Heat Transfer*, Vol. 13, No. 3, pp. 314-320.

7. Kaya, T., and Goldak J., "Numerical Analysis of Heat and Mass Transfer in Capillary Structure of a Loop Heat Pipe," *Journal of Heat and Mass Transfer*, Vol. 49, 2006, pp. 3211-3220.

8. Mishkinis, D., and Ochterbeck, J., "Homogeneous Nucleation and the Heat Pipe Boiling Limit," *Journal of Engineering Physics and Thermophysics*, Vol.76, No.4, 2003, pp. 813-818.

9. Nikitkin, M., Bienert, W., "High Power Cold Shock Phenomenon in Loop Heat Pipes," *Space Technologies and Applications International Forum*, American Institute of Physics, 2001,pp. 283-291.

10. Kaya, T., and Ku, J., "Thermal Operation Characteristics of a Small Loop Heat Pipe," *Journal of Thermophysics and Heat Transfer*, Vol. 17, No.4, 2003, pp 464-470.

11. Wirsch, P., and Thomas, S., "Performance Characteristics of Stainless Steel/ Ammonia Loop Heat Pipe," *Journal of Thermophysics and Heat Transfer*, Vol. 10, No.2, 1996, pp. 326-333.

12. Li, C., Peterson, G., and Wang, Y., "Evaporation/Boiling in Thin Capillary Wicks (I)-Wick Thickness Effects," *Journal of Heat Transfer*, Vol.128, 2006, pp. 1312-1319.

13. Li, C., and Peterson, G., "Evaporation/Boiling in Thin Capillary Wicks (II) – Effects of Volumetric Porosity and Mesh Size," *Journal of Heat Transfer*, Vol. 128, 2006, pp. 1320-1328.

14. Hanlon, M., and Ma, H., "Evaporation Heat Transfer in Sintered Porous Media," *Journal of Heat Transfer*, Vol.125, 2003, pp. 644-652.

15. Wang, Y., and Peterson, G., "Capillary Evaporation in Microchanneled Polymer Films," *Journal of Thermophysics and Heat Transfer*, Vol. 17, No. 3, 2003, pp.354-359.

16. Wang, Z., Peng, X., and Liu, T., "Visualization of Boiling Phenomenon in a Bead Packed Structure," *Experimental Heat Transfer*, Vol. 15, 2003, pp. 177-189.

17. Maydanik, Y., Vershinin, S., Korukov, M., and Ochterbeck, J., "Miniature Loop Heat Pipes---A Promising Means for Cooling Electronics," IEEE *Transactions on Components and Packaging Technology*, Vol. 28, No. 2, 2005, pp.290-296.

18. Singh, R., Akbarzadeh, A., Dixon, C., Mochizuki, M., and Reihl, R., "Miniature Loop Heat Pipe with Flat Evaporator for Cooling Computer CPU," *IEEE Transactions on Componens and Packaging Technology*, Vol. 30, No. 1, 2007, pp.42-49.

19. Wang, Y., and Peterson, G., "Investigation of a Novel Flat Heat Pipe," *Journal of Heat Transfer,* Vol. 127, 2005, pp.165-170.

20. Sauciuc, I., Mochizuki, M., Mashiko, K., Saito, Y., and Nguyen, T., "The Design and Testing of Super Fiber Heat Pipes for Electronics Cooling Applications," *Sixteenth IEEE SEMI-THERM Symposium*, San Jose, CA, 21st -23rd March 2000, pp. 27-32.

21. Tsai, M., Yu, C., and Kang, S., "Flat Plate Loop Heat Pipe with a Novel Evaporator Structure," *21st IEEE SEMI-THERM Symposium*, 15th-17th March 2005, pp. 187-190.

22. Shimizu, A., Ono, Y., and Watanabe, H., "Experimental Study on a Flexible Heat Pipe with a Carbon Fiber Arterial Wick," *Research Reports of Tokyo National College of Technology*, No. 30, 1998, pp. 9-14.

23. Savino, R., Francescantonio, N., Fortezza, R., and Abe Y., "Heat Pipes with Binary Mixtures and Inverse Marangoni Effects for Microgravity Applications," *Acta Astronautica* Vol. 61, 2007, pp. 16-26.

24. Abe, Y., Tanaka, K., Yokayama, T., and Iwasaki, A., "Heat Transfer Devices with Self Rewetting Fluids," *Proceedings of IMECE*, American Society of Mechanical Engineers, Anaheim, CA, 13th-19th November 2004-61328.

25. Abe Y., "Applications of Self-Rewetting Fluids as a Working Fluid in Heat Transfer," *The Eighteenth International Symposium on Transport Phenomena*, Daejeon, Korea, 27th -30th August 2007, pp.303-313..

26. Simoncic, B., and Rozman V., "Wettability Of Cotton Fabric By Aqueous Solutions Of Surfactants With Different Structures," *Colloids and Surfaces A: Physiochemical and Engineering Aspects*, Vol. 292, 2007, pp. 236-245.

BIOGRAPHICAL SKETCH

I completed my bachelor's studies in mechanical engineering from the Government College of Engineering, Pune (India) in 2003. I worked for a year with Cummins India Limited and went for further studies to Sweden. I obtained a Master of Science degree in 'Sustainable Energy Technology' from the Royal Institute of Technology in Stockholm. Then I came to the University of Florida in 2006 for master's studies in mechanical engineering.